NASA TECHNICAL NOTE

NASA TN D-3994

NASA TN D-3994

SPHERE BEHAVIOR AND THE MEASUREMENT OF WIND PROFILES

by James R. Scoggins

George C. Marshall Space Flight Center

Huntsville, Ala.

NATIONAL AERONAUTICS AND SPACE ADMINISTRATION • WASHINGTON, D. C. • JUNE 1967

SPHERE BEHAVIOR AND THE MEASUREMENT OF WIND PROFILES

By James R. Scoggins

George C. Marshall Space Flight Center
Huntsville, Ala.

NATIONAL AERONAUTICS AND SPACE ADMINISTRATION

For sale by the Clearinghouse for Federal Scientific and Technical Information
Springfield, Virginia 22151 – CFSTI price $3.00

TABLE OF CONTENTS

TABLE OF CONTENTS (Concluded)

LIST OF ILLUSTRATIONS

LIST OF ILLUSTRATIONS (Concluded)

LIST OF TABLES

FOREWORD

This research was submitted by the author in December 1966 as a thesis in Meteorology in partial fulfillment of the requirements for the degree of Doctor of Philosophy at the Pennsylvania State University. The author, who is a member of the Aerospace Environment Division, Aero-Astrodynamics Laboratory, NASA, Marshall Space Flight Center, attended the Pennsylvania State University under the NASA training program.

ACKNOWLEDGEMENT

I wish to express my sincere gratitude and appreciation to Dr. David F. Hoult and Dr. Hans A. Panofsky for their understanding, assistance, interest and guidance during the conduct of this investigation. My work was far more pleasant and rewarding as a result of their encouragement and support. The many helpful comments and suggestions made by Dr. Edwin F. Danielsen are greatly appreciated. Special thanks are extended to all my colleagues and associates at the NASA Marshall Space Flight Center and the Kennedy Space Center who did much to assist me during this study. They are too numerous to mention by name here, but without their help the study would not have been possible.

SPHERE BEHAVIOR AND THE MEASUREMENT OF WIND PROFILES

SUMMARY

Relatively large, smooth, superpressure, spherical balloons used to measure vertical wind profiles in the atmosphere are aerodynamically unstable and experience erratic motions when operating in the supercritical range of Reynolds numbers. These motions are larger in amplitude than the corresponding scales of atmospheric motions. These balloons cannot be used to measure a vertical wind profile accurately. The purpose of the present investigation is to answer the following questions: (1) What are the characteristics of the aerodynamic forces which cause the spurious balloon motions? (2) Can a smooth, superpressure balloon be modified to eliminate the spurious motions and provide accurate wind profile measurements?

Forces associated with aerodynamically unstable balloons were investigated by solving the equations of motion and evaluating individual force terms using high precision radar data obtained by tracking balloons as they ascended through the atmosphere. Aluminized, superpressure balloons made of 0.0127 mm (1/2 mil) Mylar with diameters of 1.22 m (4 ft), 2 m (6.56 ft), 2.13 m (7 ft), and 2.44 m (8 ft) were used. Spring-loaded valves maintained a superpressure of 600 to 800 N/m^2 (6 to 8 mbars), which was sufficient to assure sphericity even in the largest expected wind shear conditions.

As regards smooth, superpressure balloons operating in the supercritical range of Reynolds number, the following conclusions were reached: 1) Statistical properties of the spurious motions are predictable; 2) There were no systematic differences observed in the spurious motions associated with balloons of different diameters; 3) Lift and drag forces are nearly symmetrical along the horizontal axes with a mean near zero; 4) Spurious motions in the x-z and y-z planes occur with equal magnitude and frequency, and have a mean in each plane of near zero; 5) Distributions of drag coefficients are nearly symmetrical with average values between 0.25 and 0.30; 6) The drag force does not contain any preferred periods of oscillation; 7) The lift force is predominantly horizontal, increases in magnitude with balloon size, and is distributed symmetrically in the x and y directions with means near zero; 8) The lift coefficient usually varies between 0.03 and 0.05 with some values exceeding 0.07, while mean and RMS values decrease with an increase in Reynolds number in the supercritical range; 9) Below a nondimensional wave number of 0.013 the lift force is somewhat organized, but appears random at higher nondimensional

wave numbers, and; 10) There are no definite periodicities for vortex formation and separation, but shorter period changes occur with more regularity than longer period changes.

A smooth, superpressure, spherical balloon was modified to provide accurate vertical wind profile measurements. The following conclusions were reached: 1) The addition of conical, surface roughness elements 0.0762 m (3 in.) in base diameter, 0.0762 m (3 in.) high and spaced at 0.19 m (7.5 in.) apart, and a point mass of 100 g essentially eliminated the spurious motions; 2) Wind shear does not significantly influence the balloon's response capabilities since the maximum expected wind shear is small compared to the ratio of balloon ascent rate to balloon diameter; 3) The drag coefficient for the rough balloon is almost independent of Reynolds number and has a large value at all altitudes; and 4) Wind profile measurements averaged over 25- to 50-m altitude intervals can be made with an RMS accuracy of about 0.5 m/sec or less to an altitude of 18 km when the balloon is tracked by the FPS-16 radar.

INTRODUCTION

Statement of the Problem

Balloons are used extensively to measure vertical wind velocity profiles in the atmosphere. Altitude and wind speed resolution are dependent upon balloon properties such as mass and its distribution, shape, size and surface roughness, and upon the capability of the system used to track the balloon. Relatively large, e.g., 2-m diameter, smooth, superpressure spheres experience spurious oscillations as they rise even through calm air [1, 2]. Spurious motions are also observed when these balloons rise through the atmosphere, making it impossible to measure true wind motions on a small scale. Measurements of small-scale changes in the horizontal wind along the vertical axis are needed in the design and operation of space vehicles, and in meteorological problems such as turbulent diffusion, clear air turbulence, energy transfer, wave motion and forecasting.

The purpose of this study is to investigate the forces on superpressure, spherical balloons which cause spurious oscillations, and to develop an aerodynamically stable, spherical balloon wind sensor capable of providing accurate small-scale wind measurements to an altitude of 18 km.

Review of Previous Studies

Reynolds number and drag are commonly used as parameters in investigations of sphere motion [3, 4]. The Reynolds number for a sphere is defined as $\frac{\rho |\vec{V}| d}{\mu}$ where ρ is fluid density, V the velocity relative to the sphere, d the diameter of the sphere, and μ the coefficient of viscosity of the fluid. Drag is defined as $\frac{1}{2} \rho C_D A |\vec{V}| \vec{V}$ where C_D is the drag coefficient and A is the cross-sectional area of the sphere. At small Reynolds number, transition and flow separation takes place near the equator of a sphere, resulting in a large eddying wake. The boundary layer upstream of the point of separation is laminar. As Reynolds number is increased, transition from laminar to turbulent flow and the separation point move downstream, resulting in reduced wake and drag. These facts are fundamental to almost all investigations relating to spheres.

Bacon and Reid [5] summarize previous work on sphere motions and drag up to that time. Most investigations had been conducted in wind tunnels, and it was found that the type of support such as pendulum, back spindle, wires, etc., influenced greatly the results obtained. Results obtained from hydrogen-filled rubber balloons rising in calm air were even more irregular than those obtained in tunnels. Drag curves obtained by different investigators were not consistent. A satisfactory explanation of the differences had not been given. Bacon and Reid investigated the influence of various factors such as tunnel turbulence, sphere support, etc., in an attempt to account for the discrepancies. Spheres were dropped in air for the purpose of correlating with tunnel data. The spheres were dropped from an altitude of 610 m (2000 ft) during very light wind conditions and tracked by theodolites. Among other types, rubber balls 0.305 m (1 ft) in diameter were used. Highly erratic data were obtained which were attributed to a patch on the surface of the sphere. The patch caused a noticeable increase in drag. Polished wood spheres 30.5 to 38.1 cm (12 to 15 in.) in diameter were also used; these gave consistent results for Reynolds numbers up to 1.5×10^6. No information was given on the density of these spheres.

Bacon and Reid pointed out that, even though the Reynolds numbers were equal for two geometrically similar objects, the Reynolds number of the tunnel itself changes with velocity, and it is impossible to get complete dynamic similarity because the airflow is not geometrically similar when referred to the dimensions of the spheres. It was found that turbulence had a pronounced effect on similarity conditions. Consistent results between wind tunnel and falling sphere data were

not obtained. In comparing falling-sphere and tunnel data, Bacon and Reid concluded that tests in free air demonstrated that existing wind tunnels could not simulate turbulence conditions prevailing in the atmosphere.

Hoerner [6] further investigated the influence of support methods in wind tunnels on the drag of spheres and, in addition, investigated the effects of surface roughness. He found that surface roughness had a decisive effect on sphere turbulence measurements particularly at supercritical Reynolds numbers, and that it was necessary to use accurately designed and highly polished spheres in making turbulence measurements. He concluded that at supercritical Reynolds numbers the degree of surface roughness was far more important than Reynolds number effects in determining drag. Hoerner also found that surface roughness composed of grains of sand caused the transition (critical) Reynolds number to decrease, and that the drag becomes independent of the Reynolds number for very rough spheres.

Platt [7] extended the work on spheres in wind tunnels, using spheres of several sizes and wind tunnels of different types. He correlated drag with pressure variations over the sphere. This work was extended even further by Dryden, et al. [8, 9] by consideration of a new variable, viz., the scale of turbulence. Hot wire anemometers and spheres were used to measure turbulence in tunnels. It was concluded that the critical Reynolds number of spheres depends on the scale of turbulence as well as its intensity.

Roshko [10] studied the wake behind 2-dimensional bluff bodies. He considered relationships between the wake and the body including wake scale, frequencies, energy and interference between wakes. Experiments were conducted in a 50.7- by 50.7-cm (20 in.) low-turbulence wind tunnel at the California Institute of Technology to investigate coupling between the wake and potential flow immediately behind bluff cylinders. He found large pressure fluctuations about two plate widths behind plates in the region where vortices form alternately. He demonstrated that vortex dynamics had a strong effect on the base pressure behind a circular cylinder by using a splitter plate to inhibit vortex formation. Although Roshko's work contributed greatly to the understanding of the relationships between bodies and properties of their wakes, empirical relations were still required.

Fung [11] studied lift and drag forces on circular cylinders at supercritical Reynolds numbers. Experiments were conducted in a tunnel using a cylinder approximately 0.305 m (1 ft) in diameter and 1.83 m (6 ft) long. Lift is the force in the direction perpendicular to the velocity vector, and drag is parallel to the velocity vector. He observed that the lift and fluctuating part of

the drag were random phenomena. He found that, in general, the variation from the mean did not exceed 7 percent, but on occasions it reached 15 percent. The lift coefficient curve for a cylinder taken from Fung's work is shown in Figure 1.

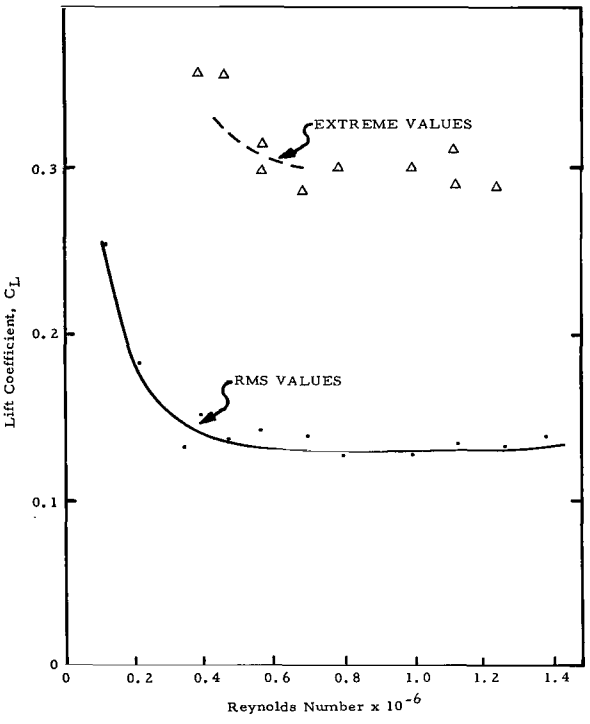

FIGURE 1. THE AMPLITUDE OF THE LIFT COEFFICIENT FOR A FIXED CYLINDER (AFTER FUNG)

Fung performed a power spectrum analysis of the lift force which is a random function of time. The power spectra varied from sample to sample, but the spectra were not found to vary significantly with Reynolds number in the supercritical range. There were no large peaks observed in the spectra. A similar analysis was performed for the drag force with peaks appearing in the spectra near a Strouhal number ($\frac{nd}{v}$; n = cycles/sec, d = diameter of cylinder, v = velocity) of 0.3. Fung concludes by stating that the most important feature of the forces induced on a circular cylinder by vortex shedding in the supercritical Reynolds number range is the randomness. He further concludes that the mechanism of vortex shedding is poorly understood and defies theoretical treatment although Roshko's work opens up new vistas of research.

Using expandable neoprene balloons of different sizes and weights, Killen [1] performed experiments in a large hangar where the wind was calm. Some of the balloons had a weight attached to simulate a meteorological instrument package usually carried aloft by balloons, while others had nothing attached. All the balloons ascended in an erratic fashion and without consistency between runs. In some cases, after terminal velocity was reached, the balloons appeared to oscillate about the vertical axis, while in other cases their distance from the vertical axis increased with altitude. There were no systematic motions observed. Killen concluded that aerodynamic lift forces were responsible for the observed horizontal motions, and that small-scale changes in the horizontal wind field could not be accurately measured by balloons. Similar tests by Murrow and Henry [2] in the same or similar hangar confirmed Killen's results.

Preukschat [12] investigated the motion of rising and falling spheres. He found that the wavy motions of a rising sphere became more significant as the density ratio (density of sphere to that of the liquid) decreased. The motions resulted from a low mass-to-force ratio where the force resulted from non-symmetrical vortex shedding. Rising spheres were observed to follow a 2-dimensional wavy path which sometimes changed into helical motion. A distinct wave length was found for both types of motion and a Strouhal number of 0.05 calculated which is about 3 times smaller than that for circular cylinders. For low density ratios, the drag coefficient scattered randomly about a mean value, but as the density ratio approached 0.93, the drag coefficient approached the steady-state value independently of Reynolds number.

MacCready and Jex [13] performed experiments with spheres rising and falling in air and water. They found that sphere motions depend directly on Reynolds number, relative mass of the sphere to the displaced fluid (density ratio), rotational inertia, surface roughness, sphericity, and random orientation. Preukschat's conclusion that the amplitude of the lateral motions increases as the density ratio decreases was confirmed. Fairly regular zigzag or spiral motions were observed at subcritical Reynolds numbers where the wake separation is laminar. Wave lengths of about 12 times the diameter of the sphere were observed. At supercritical Reynolds numbers where the wake separation is turbulent and the wake smaller, an irregular spiral was observed. MacCready and Jex concluded that spherical balloons operating in the subcritical Reynolds number range, and at higher Reynolds numbers with the addition of surface roughness elements, are good wind sensors, although limits of the capabilities for such balloons were not given.

Leviton [14] proposed that a 2-m diameter, smooth, superpressure sphere be used to make detailed vertical wind profile measurements. The FPS-16 high precision radar would be used for tracking the sphere. Leviton concluded that wind speeds averaged over about 30 m altitude could be measured with an RMS accuracy of 0.3 to 1.0 m/sec. Scoggins [15, 16], MacCready and Jex [13], and Rogers and Camitz [17] investigated the behavior of smooth, superpressure balloons and found that it is impossible to make accurate wind measurements using such balloons in the supercritical Reynolds number range because of their erratic behavior associated with vortex shedding. Scoggins [15] proposed a solution by adding large, conical, surface roughness elements to control vortex formation and separation thus stabilizing the wake, and by attaching a small point mass to provide rotational stability and increase the density ratio. Initial experiments of what is now called the "Jimsphere" were conducted by Scoggins, and results later confirmed by Reid [18], MacCready and Jex [13], and

Rogers and Camitz [17]. Rogers and Camitz, observing motions of the Jimsphere with Doppler radar, found a systematic oscillation with a period of 4.5 sec. This oscillation is almost entirely removed by the data reduction procedure employed by Scoggins [19].

Eckstrom [20] developed fabrication techniques and performed a rather comprehensive investigation of the Jimsphere and its response capabilities. Drag coefficient curves were determined from wind tunnel experiments. The drag coefficient was found to be essentially independent of Reynolds number confirming calculations by Scoggins [16]. Eckstrom determined the theoretical response of the Jimsphere and concluded that it was capable of sensing wind motions with dimensions of only a few meters.

Origin and Importance of the Present Study

Studies began in 1961 to develop a system for making improved wind profile measurements by Jiusto [21] and Figge, et al. [22]. While these studies were not entirely successful, another program by Henry, et al. [23], employing a smoke producing rocket and cameras, provided wind profile measurements of the required accuracy and altitude resolution. The smoke trail method turned out to be too expensive (about $3000 per velocity profile) for operational use, dependent on good weather conditions, and required extensive data reduction procedures. The present study to develop an accurate balloon wind sensor began in 1963 after it was realized that the above methods were unsatisfactory. Full-scale flight data using balloons of different configurations were obtained by Scoggins [15] at the NASA Marshall Space Flight Center, Huntsville, Alabama, and at the Kennedy Space Center, Florida. Data obtained by tracking the balloons with an FPS-16 high precision radar form the primary data source for the present investigation. Experimental measurements by radar were restricted to the Kennedy Space Center. The spherical balloon wind sensor developed as a result of the present investigation has been in routine use at the two major national test ranges since late 1964. Some of the measurements have been published by Scoggins and Susko [24].

Small-scale motions may cause excitation of dynamic bending modes, fuel slosh, and the control system of large space vehicles [25]. Geissler [26] presented control laws for the Saturn space vehicle which may be used to alleviate some of the wind effects; however, atmospheric winds remain perhaps the single most important meteorological factor in the design and operation of space vehicles. In fact, the establishment of an optimum control law requires

a knowledge of the spectral composition of the wind field. Improved wind velocity profile measurements are badly needed in various areas of meteorological research. Danielsen [27], Weinstein, et al. [28], Endlich [29], and others have conducted meteorological research employing small-scale wind measurements of the type provided by the wind sensor developed as a result of the present study. These measurements are expected to continue to be used in fundamental investigations of space vehicle response and meteorological research.

EQUATIONS OF MOTION OF A RISING SPHERICAL BALLOON

Unstable Balloon

When a relatively large, smooth, superpressure balloon ascends through the lower atmosphere, the Reynolds numbers are in the supercritical range. The boundary layer is turbulent, and the separation point is downstream near the back of the sphere thus producing a wake with a small diameter. Separation does not occur at the same points around the sphere at all times because of build-up and decay of vortices or tripping of the boundary layer by surface irregularities. Presumably, the wake meanders around on the back of the sphere producing forces which cause erratic motions as the balloon ascends. In this section it is assumed that the balloon moves through a calm atmosphere so that all motions of the balloon relative to the air are identical to those measured relative to a fixed point on the earth.

An ascending balloon experiences drag, lift, buoyancy, gravity, and pressure forces. The variation of pressure over the surface of an accelerating sphere results in a force which acts as an inertia force if the balloon is imparting momentum to the air, and acts as an accelerating force when the air is imparting momentum to the balloon. The magnitude of this force is given by the product of one half the mass of the displaced fluid (apparent mass) and the acceleration of the balloon [30]. As a sphere moves through an ideal fluid, the momentum of the fluid is increased in all directions from the sphere to a distance of several sphere diameters, diminishing from the sphere outwards. Essentially the same flow field surrounds a sphere moving through a real fluid except that a wake forms behind the sphere. Assuming the wake to be a cylinder extending to infinity with a diameter equal to that of the sphere, the momentum computed from ideal fluid theory in this cylinder was found to be approximately 4 to 5 percent of the total momentum imparted to the fluid. This is the largest wake

expected; therefore, the apparent mass may be treated as constant. Moreover, because of symmetry, the apparent mass associated with a sphere is a scalar quantity. In a calm atmosphere the balloon imparts momentum to the air so that the apparent mass term acts to increase the inertia of the balloon and may be considered as part of the mass of the system.

From Newton's second law of motion

$$(M + M_A)\,\dot{\vec{V}}_B = \Sigma\vec{F} = \vec{B} + \vec{L} + \vec{D}. \tag{1}$$

After substitution for the forces, this equation becomes

$$(M + M_A)\,\dot{\vec{V}}_B = \vec{g}[\,VOL(\rho_g - \rho_a) + M_B] + \tfrac{1}{2}\rho_a C_L A\,|\vec{V}|\,(\vec{V}\times\vec{n}) + \tfrac{1}{2}\rho_a C_D A\,|\vec{V}|\,\vec{V}, \tag{2}$$

where M = mass of the balloon and gas

M_A = apparent mass

M_B = mass of balloon

VOL = volume of balloon

A = cross-sectional area of balloon

ρ_a = density of air

ρ_g = density of gas

$\vec{V}$ = velocity of air relative to the balloon

$\dot{\vec{V}}_B$ = acceleration of the balloon

C_D = drag coefficient

C_L = lift coefficient

$\vec{g}$ = acceleration of gravity

$\vec{n}$ = a unit vector perpendicular to $\vec{V}$ and in the plane of the lift force.

The first term on the right-hand side of equation (2) contains buoyancy and gravity; however, these forces will be treated jointly. These forces always act in the vertical direction. The second and third terms on the right-hand side of equation (2), lift and drag forces, respectively, act in perpendicular directions with drag being defined as having a direction along the relative velocity vector. The lift force may assume any direction in the plane perpendicular to the drag vector.

Equation (2) may be written in component form for a three-dimensional orthogonal coordinate system. The coordinate system used in this report assumes a flat earth with x positive toward the east, y positive toward the north, and z positive upward. In this coordinate system the component equations of equation (2) are:

x-component

$$(M+M_A)\dot{V}_{Bx} = \tfrac{1}{2}\rho_a C_L A|\vec{V}|(\vec{V}\times\vec{n})\cdot\vec{i} + \tfrac{1}{2}\rho_a C_D A|\vec{V}|V_x \tag{3}$$

y-component

$$(M+M_A)\dot{V}_{By} = \tfrac{1}{2}\rho_a C_L A|\vec{V}|(\vec{V}\times\vec{n})\cdot\vec{j} + \tfrac{1}{2}\rho_a C_D A|\vec{V}|V_y \tag{4}$$

z-component

$$(M+M_A)\dot{V}_{Bz} = g[VOL(\rho_g-\rho_a)+M_B] + \tfrac{1}{2}\rho_a C_L A|\vec{V}|(\vec{V}\times\vec{n})\cdot\vec{k} + \tfrac{1}{2}\rho_a C_D A|\vec{V}|V_z \tag{5}$$

Along the x, y, and z axes, respectively, $\vec{i}$, $\vec{j}$, and $\vec{k}$ are unit vectors.

The component forces are considered positive when they point in the positive direction along the axes. The vector lift force is perpendicular to the vector drag which restricts it to a particular plane at a given instant of time, but does not restrict its direction within that plane. Thus, the direction of the component lift forces and, therefore, that of the vector lift force as well, must be such that equations (2) through (5) balance.

The equations of motion for an unstable balloon rising through a changing wind field will not be considered here. Balloon motions caused by unstable lift forces are generally an order of magnitude larger than true small-scale atmospheric motions (over altitude layers of less than approximately 300 m) and, therefore, it is not possible to measure these motions with an unstable balloon.

Stable Balloon

A stable balloon is by definition one that rises vertically along a straight line in a calm atmosphere. The lift forces are zero, and the only forces acting on the balloon are buoyancy (defined to include gravity) and drag. The vector equation of motion is

$$(M + M_A)\dot{\vec{V}}_B = \vec{g}[\,VOL(\rho_g - \rho_a) + M_B] + \tfrac{1}{2}\rho_a C_D A\,|\vec{V}|\,\vec{V} \tag{6}$$

which may also be written as

$$(M + M_A)\dot{V}_{Bz} = g[\,VOL(\rho_g - \rho_a) + M_B] + \tfrac{1}{2}\rho_a C_D A\,|\vec{V}|\,V_z\,, \tag{7}$$

since there is no motion in the horizontal directions. These equations are valid only for a stable balloon rising through a calm atmosphere in which case the balloon imparts momentum to the atmosphere, and the apparent mass term acts to increase the inertia of the system.

We now consider a stable balloon rising through a changing wind field. The vector equation of motion is

$$M\dot{\vec{V}}_B = \vec{g}[\,VOL(\rho_g - \rho_a) + M_B] + \tfrac{1}{2}\rho_a C_D A\,|\vec{V}|\,\vec{V} - M_A\,\dot{\vec{V}}. \tag{8}$$

The apparent mass term has been separated from the inertia term since momentum may be transferred from the balloon to the air or vice versa. If momentum is transferred from the balloon to the air, the last term in equation (8) will act as an inertia term, but if momentum is transferred from the air to the balloon, this term acts to accelerate the balloon.

OBSERVED AERODYNAMIC CHARACTERISTICS OF SMOOTH SUPER-PRESSURE BALLOON WIND SENSORS RISING FREELY IN THE ATMOSPHERE

Description of the Wind Sensors

In meteorology, as well as in the design of space vehicles, it is desirable to obtain accurate wind measurements to an altitude of at least 15 to 20 km and, in some cases, to a much higher altitude. In order to obtain wind measurements

to a given (maximum) altitude, the balloon wind sensor required is a function of its buoyancy-to-weight ratio. For a sphere made of a given material, the larger the diameter, the higher will be its floating altitude. However, it is more difficult to launch larger balloons especially during high winds. It is generally better to use a balloon no larger than required to reach the desired altitude.

A 2-m diameter, superpressure sphere made of $\frac{1}{2}$ mil, aluminized mylar with two release valves and one fill valve made of plastic, weighs approximately 300 grams and will float at an altitude in excess of 20 km when inflated with helium. A sphere of this type is shown in Figure 2. The pressure release valves are spring-loaded and maintain a superpressure of approximately 600 to 800 N/m^2 (6 to 8 mbars). The balloon is used as a passive target and there is no instrumentation attached.

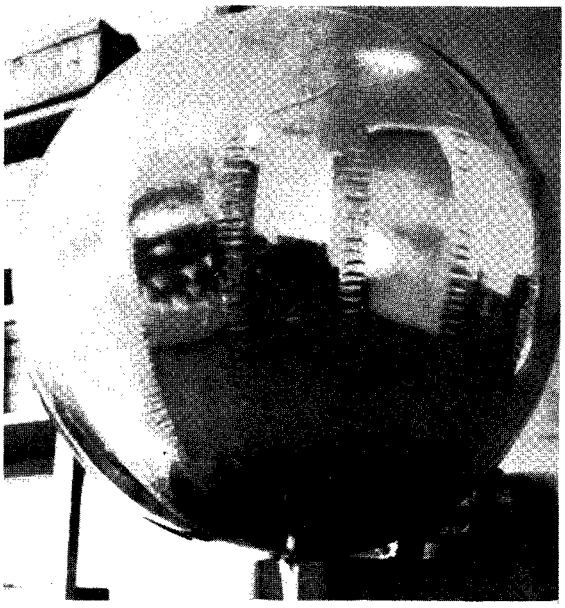

FIGURE 2. SMOOTH SUPERPRESSURE SPHERE

Observed Spurious Motions and Their Dependence on Reynolds Number

A series of measurements made at approximately 1-hour intervals with a 2-m diameter sphere of the type described above as the wind sensor is shown in Figure 3. The balloons were tracked with the FPS-16 radar. These measurements were made at Cape Kennedy, Florida, on January 3, 1961. The data reduction method used to compute wind velocity from radar position data is given in Appendix A. The solid line superimposed on the dotted profile represents the wind profile measured by the rawinsonde system. This profile represents winds averaged over approximately 600 m and is shown for comparison only.

At high Reynolds numbers the boundary layer associated with the balloon is turbulent while at low Reynolds numbers the boundary layer is laminar. Reynolds numbers are called supercritical in the turbulent flow regime, and subcritical in the laminar flow regime. At supercritical Reynolds numbers, flow separation takes place on a small area near the back of the sphere resulting

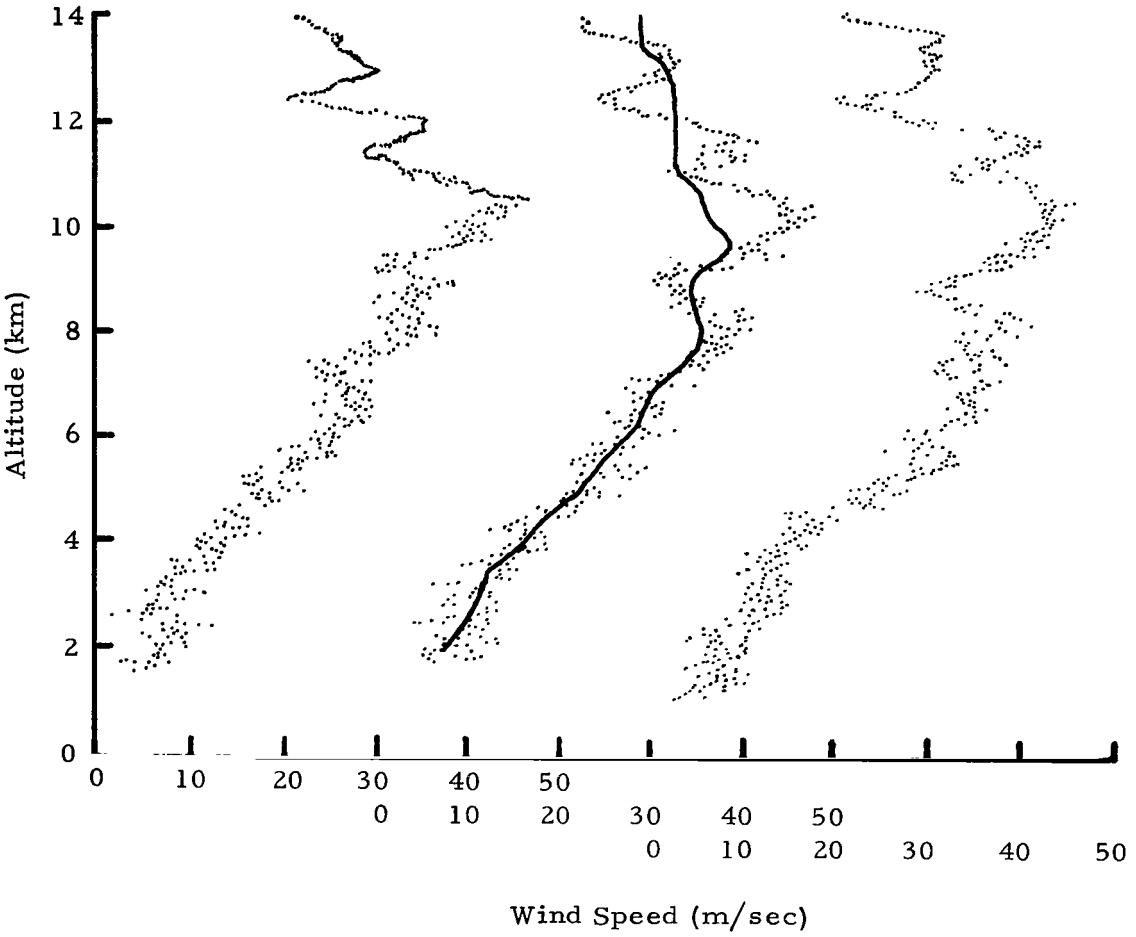

FIGURE 3. SCALAR WIND SPEED PROFILES MEASURED AT APPROXIMATELY 1-HOUR INTERVALS USING SMOOTH, 2-m DIAMETER SUPERPRESSURE BALLOON (SOLID LINE IS RAWINSONDE MEASURED PROFILE)

in a small wake. As vortices build up and separate, the separation region moves around on the back of the sphere, causing the wake to tilt. Tilting of the wake, in turn, causes lift forces which are responsible for the observed spurious motions. At subcritical Reynolds numbers, flow separation takes place farther upstream (near the sphere's equator), resulting in a large wake. In this case the formation and separation of vortices do not cause the wake to tilt significantly, so the lift forces are much smaller than the drag forces. Thus, at subcritical Reynolds numbers a sphere is aerodynamically more stable than at supercritical Reynolds numbers.

In Figure 3 the motions of the balloon are observed to be erratic to an altitude of approximately 12 km, and above this altitude the erratic behavior disappears. It is at this altitude that the flow regime for the 2-m diameter sphere used experiences transition from a supercritical (turbulent boundary layer) to a subcritical (laminar boundary layer) flow regime. Coincident with this transition, the turbulent wake associated with the sphere increases in size and becomes more stable. Thus, at subcritical Reynolds numbers the lift forces are drastically reduced in magnitude, the drag force becomes larger and more stable, and the balloon becomes a better wind sensor.

EVALUATION OF THE EQUATIONS OF MOTION FOR SMOOTH SUPERPRESSURE BALLOONS FROM EXPERIMENTAL DATA

Solution of the Equations

A solution of equations (2) through (5) and evaluation from experimental data provide an improved understanding of the forces which act upon a rising, aerodynamically unstable spherical balloon and which produce spurious or self-induced motions. The spurious motions were determined by defining the "true" motions of the balloon by use of a numerical filter function (see next section), then subtracting these motions from the measured motions. Since the spurious balloon motions are several times larger than atmospheric motions on the same scale as shown from measurements by independent methods, the definition of the filter function is not too critical. The filter function could be replaced by a moving arithmetic average without degrading the results.

With the assumption of no vertical air motion, the motion of the balloon relative to the air is given by the vector sum of the ascent rate of the balloon and the horizontal components of the spurious motions. Spurious motions in the vertical direction are small compared to the ascent rate and are neglected. Accelerations of the balloon were calculated from the measured speeds for the x, y and z directions. Accelerations computed from the spurious balloon motions defined above were almost identical to those computed directly from the measured speeds. This is because acceleration caused by spurious balloon motions are an order of magnitude larger than those caused by a change of true wind speeds which the balloon experiences as it rises. Using the measured accelerations, the sum of the forces acting along each axis was determined and then resolved into individual force components.

Density, ρ, apparent mass, M_A, buoyancy, B, and the sum of the forces along each axis, F_x, F_y, and F_z, were computed as follows:

$$\rho = \frac{M_w p}{R^* T} \tag{9}$$

$$M_A = \frac{2}{3} \pi r^3 \rho_a \tag{10}$$

$$B = g[\frac{4}{3} \pi r^3 (\rho_g - \rho_a) + M] \tag{11}$$

$$F_x = \dot{V}_x (M + M_A) \tag{12}$$

$$F_y = \dot{V}_y (M + M_A) \tag{13}$$

$$F_z = \dot{V}_z (M + M_A) + B \tag{14}$$

where r is radius of the sphere, T is temperature, M_w is molecular weight, R^* is the universal gas constant, and p is pressure. Pressure and temperature are obtained from radiosonde flights.

The coordinate system used and an illustration of the resolution of the velocity vector into its components are shown in Figure 4. Except for signs, the direction of the measured velocity vector may be replaced by the direction of the drag force vector since the drag vector is defined as being opposite the measured velocity vector. The following relationships are obtained directly from Figure 4:

$$\cos\phi = \frac{V_H}{|\vec{V}|}, \quad \cos\theta = \frac{V_x}{V_H}. \tag{15}$$

Solving for V_x we get

$$V_x = |\vec{V}| \cos\phi \cos\theta, \tag{16}$$

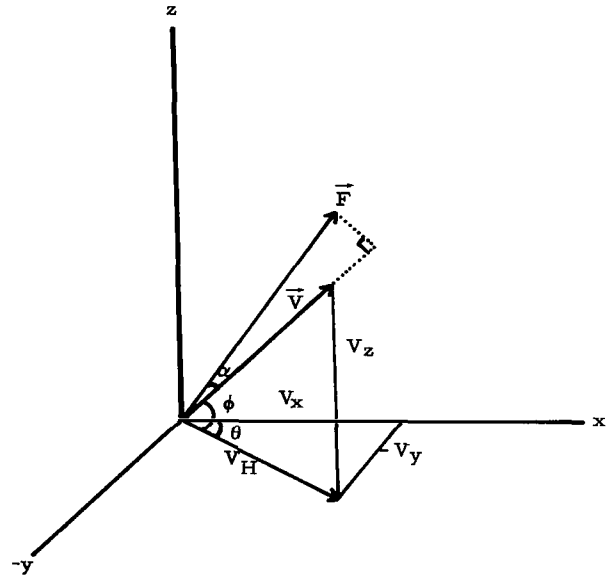

FIGURE 4. COORDINATE AXIS SHOWING RESOLUTION OF WIND VECTOR AND THE RELATIONSHIP BETWEEN FORCE AND WIND VECTORS

where

$$|\vec{V}| = [V_x^2 + V_y^2 + V_z^2]^{\frac{1}{2}} .$$

The expression $\vec{V}$ may be replaced by $-\vec{D}$ and V_x by D_x. Since ϕ and θ are determined by the component wind speeds, equation (15) may be substituted into equation (16) giving

$$D_x = -|\vec{D}| \cos\phi \cos\theta = -|\vec{D}| \left(\frac{V_H}{|\vec{V}|}\right)\left(\frac{V_X}{V_H}\right) = -|\vec{D}| \frac{V_x}{|\vec{V}|} . \tag{17}$$

Similarly, equations for the drag force components in the y and z directions are given by

$$D_y = -|\vec{D}| \frac{V_y}{|\vec{V}|} \tag{18}$$

and

$$D_z = -|\vec{D}| \frac{V_z}{|\vec{V}|} . \tag{19}$$

The magnitude of the drag force, $|\vec{D}|$, is given by

$$|\vec{D}| = |\vec{F}| \cos\alpha = [D_x^2 + D_y^2 + D_z^2]^{\frac{1}{2}} \tag{20}$$

where

$$\cos\alpha = \frac{F_x V_x + F_y V_y + F_z V_z}{|\vec{F}|\ |\vec{V}|} \tag{21}$$

and

$$|\vec{F}| = [F_x^2 + F_y^2 + F_z^2]^{\frac{1}{2}} .$$

The term α is defined as the angle between $\vec{F}$ and $\vec{V}$, and is a function of the magnitude of the lift force (see Figure 4).

The lift force components are given by

$$L_x = F_x - D_x \tag{22}$$

$$L_y = F_y - D_y \tag{23}$$

$$L_z = F_z - D_z \tag{24}$$

and the magnitude of the lift force, $|\vec{L}|$, and the horizontal component of the lift force, L_H, by

$$|\vec{L}| = [L_x^2 + L_y^2 + L_z^2]^{\frac{1}{2}} \tag{25}$$

and

$$L_H = [L_x^2 + L_y^2]^{\frac{1}{2}} . \tag{26}$$

The direction of the horizontal lift force, Ψ, is given by

$$\Psi = \tan^{-1} \frac{|L_y|}{|L_x|} + \text{quadrant correction}, \tag{27}$$

where the quadrant correction is determined by the signs of L_y and L_x.

The drag and lift coefficients, C_D and C_L, respectively, are given by

$$C_D = \frac{2|\vec{D}|}{\pi \rho_a r^2 |\vec{V}|^2} \tag{28}$$

and

$$C_L = \frac{2|\vec{L}|}{\pi \rho_a r^2 |\vec{V}|^2} . \tag{29}$$

Characteristics of the Forces

Analysis of many ascents of superpressure, spherical balloons which have a smooth surface and are aerodynamically unstable at supercritical Reynolds numbers, show that only the statistics (means, variances, etc.) of self-induced or spurious motions are predictable. Spiral, planar, and random motions have been observed from balloons rising in the atmosphere as well as from spheres rising or falling in water, but with no regularity [13]. The types of motion observed appear to be a function of the formation and separation of vortices which are random events. Vortex formation and shedding phenomena associated with flow around cylinders show similar results in the supercritical flow regime [11]. Because of the random nature of the spurious motions and thus of the forces associated with aerodynamically unstable balloons, statistical methods (empirical probability distributions and spectra) are used to investigate the behavior and interrelationships of the forces acting on the rising balloons.

The average ascent rate of balloons rising in the atmosphere in the supercritical flow regime is essentially constant. The balloons are tracked in space as a function of time, and velocities computed as a function of altitude (Appendix A). Because of the relatively constant ascent rate, it is possible to relate space and time through the relationship $V_z \Delta t = \Delta Z$. For example, wave number spectra may be converted to frequency spectra and vice versa.

In the analysis which follows, balloons with diameters of 1.22 m (4 ft), 2 m (6.56 ft), 2.14 m (7 ft), and 2.44 m (8 ft) are used. These are designated as tests 1761, 1762, 1767, and 1768, respectively. All measurements were made on the same day at Cape Kennedy, Florida. The same FPS-16 radar was used to track the balloons. The balloons were all made of 0.0127 mm ($\frac{1}{2}$ mil), aluminized Mylar and inflated with helium. The superpressure of 600 to 800 N/m^2 (6 to 8 mbars) is sufficient to maintain sphericity even in large shear layers. The 1.22-m (4-ft) diameter sphere goes from supercritical to subcritical Reynolds numbers at an altitude near 5 km, and the larger balloons near 13 km. Spurious motions are analyzed below these altitudes for the respective balloons.

Because of the symmetry of a spherical balloon, statistical properties of the erratic motions in the horizontal plane should be independent of direction. This was verified along the x (x - z plane) and y (y - z plane) axes. In the analysis that follows, data are given only for the y-axis. Wind shears are an order of magnitude smaller than V_{Bz}/d and would not be expected to significantly

influence the spurious motions of the balloons. Superpressure balloons of different sizes rising through the atmosphere give similar results in the supercritical flow regime. This is because of Reynolds number similarity, which means that characteristics of the flow over the balloons are independent of viscosity.

Composite Forces. Composite forces represent the sum of all forces acting on the balloon along a given axis. These forces, which include the effects of apparent mass, were computed using equations (12) through (14). The magnitude of the inertia term in equation (14) is small compared with buoyancy; therefore, the composite force in the z-direction is essentially equal in magnitude to buoyancy, which is treated in a later section.

Probability distributions of the composite forces along the y-axis are shown in Figure 5 for the four balloons. All forces have been normalized by

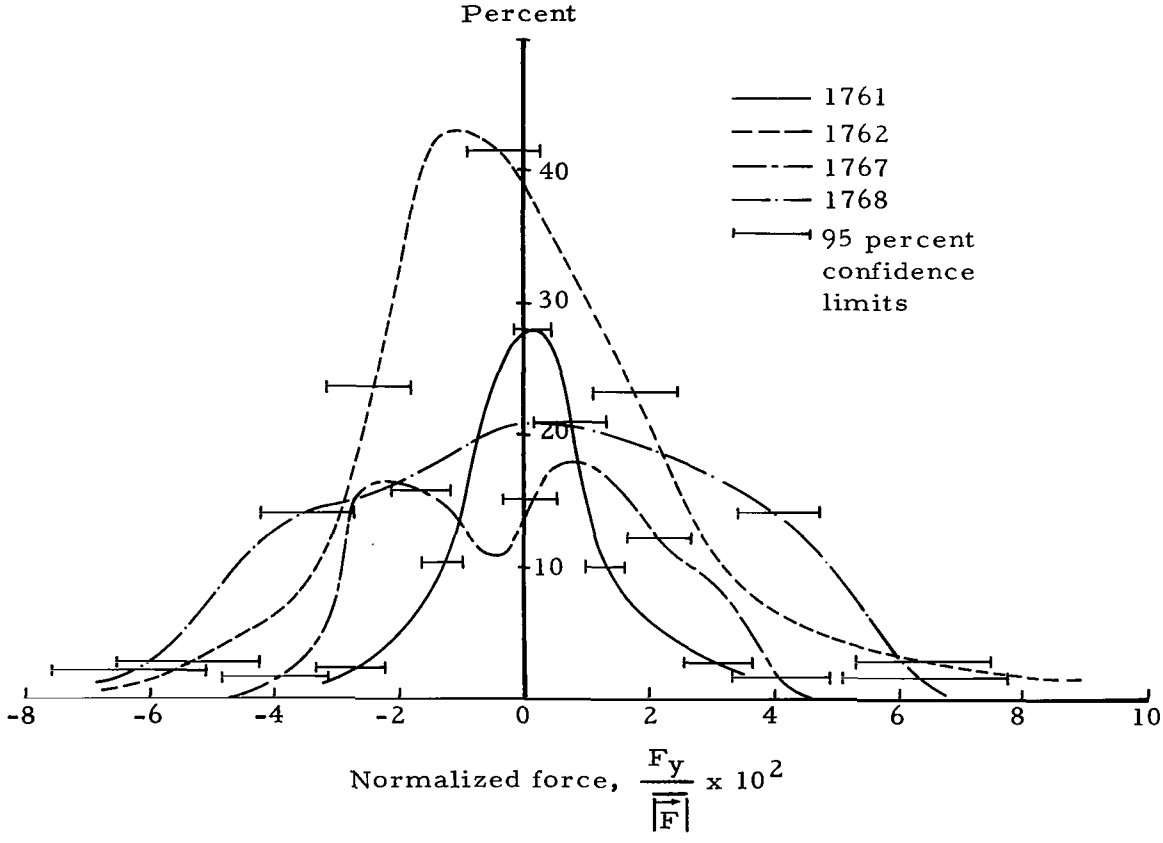

FIGURE 5. PROBABILITY DISTRIBUTIONS OF NORMALIZED COMPOSITE FORCES ALONG y-AXIS

$|\overrightarrow{F}|$. Cumulative frequency distributions or ogives corresponding to these distributions and plotted on probability paper are shown in Figure 6. The distributions are normal or Gaussian as indicated by the straight lines and the 95 percent

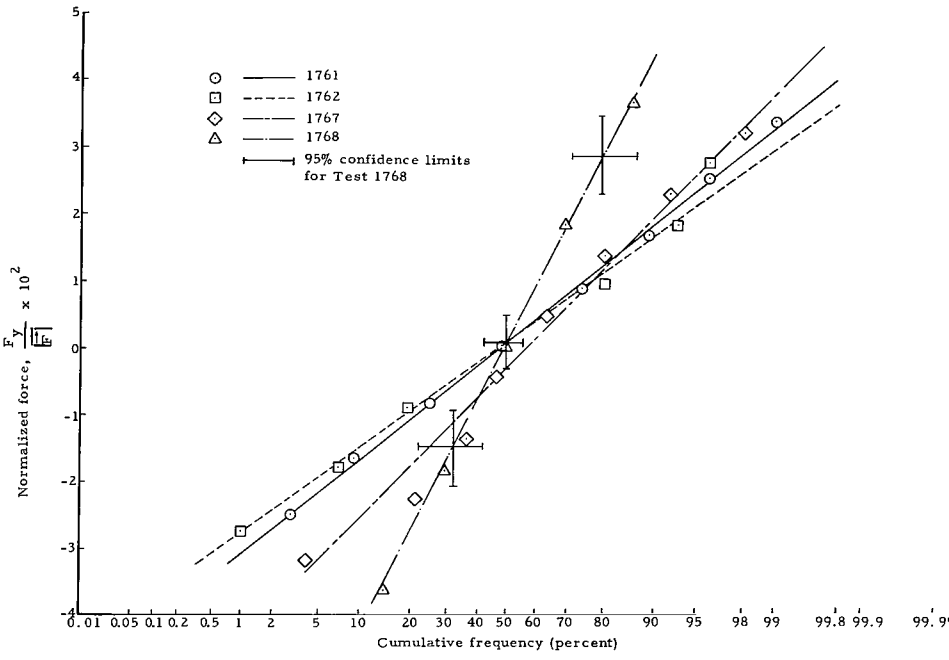

FIGURE 6. CUMULATIVE FREQUENCY DISTRIBUTIONS (OR OGIVES) OF NORMALIZED COMPOSITE FORCES ALONG y-AXIS

confidence limits. The method for computing confidence limits for a cumulative frequency distribution, assuming the theoretical distribution is normal (Gaussian), is given by Hald [31]. The 95 percent confidence limits were computed at approximately the mean, ± 1 standard deviation, and ± 2 standard deviations for each cumulative frequency distribution. These limits were then transferred to the probability distributions via the scale of the variable since it is common to both figures. This is not a common statistical procedure, but it does provide an indication of how much the probability distributions can vary and still remain

within the 95 percent confidence limits. The 95 percent confidence limits are shown on all probability distributions.

The probability distributions of the composite forces are nearly symmetrical with a mean near zero. This indicates that the spurious motions, which primarily determine the accelerations over small altitude intervals, are also symmetrical; i. e., the balloon oscillates back and forth about its mean path as it rises through the atmosphere.

Individual Force Terms

Buoyancy. Buoyancy is defined as the net upward force due to the difference in densities between the balloon system (including gas) and the air. It is convenient to consider gravity in this term since it acts in the vertical and does not appear in any of the other terms. At lower altitudes, buoyancy is a large force which decreases with altitude as the air density decreases. Floating altitude is reached when the buoyancy force becomes zero.

Drag. Probability distributions of the y-components of the drag force given by equation (18) are shown in Figure 7. Probability distributions

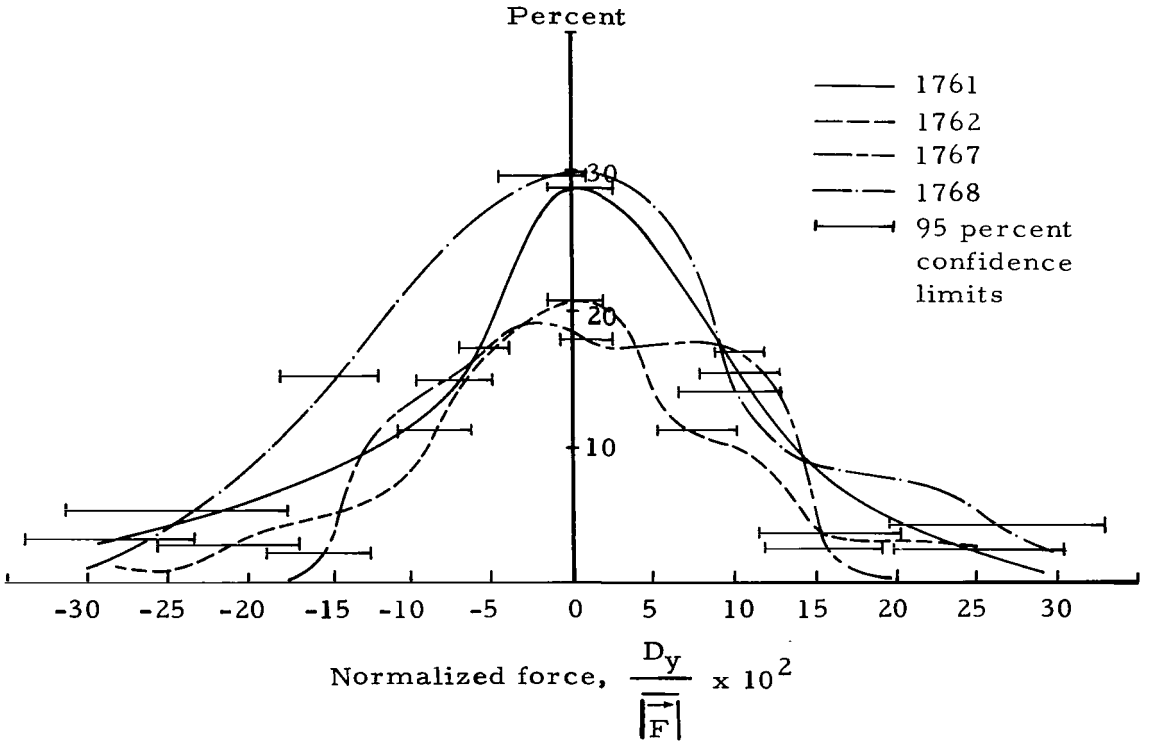

FIGURE 7. PROBABILITY DISTRIBUTIONS OF NORMALIZED DRAG FORCES ALONG y-AXIS

of the forces in the x-direction were similar to those in the y-direction. The vertical component of the drag force decreases in magnitude with altitude and becomes zero at the floating altitude. The magnitude of the vertical component of drag is an order of magnitude greater than the magnitudes of the horizontal components. This is caused by the greater component of velocity relative to the balloon in the z-direction.

Figure 8 shows probability distributions of the drag coefficients. The distributions are reasonably symmetrical with the average value of the drag

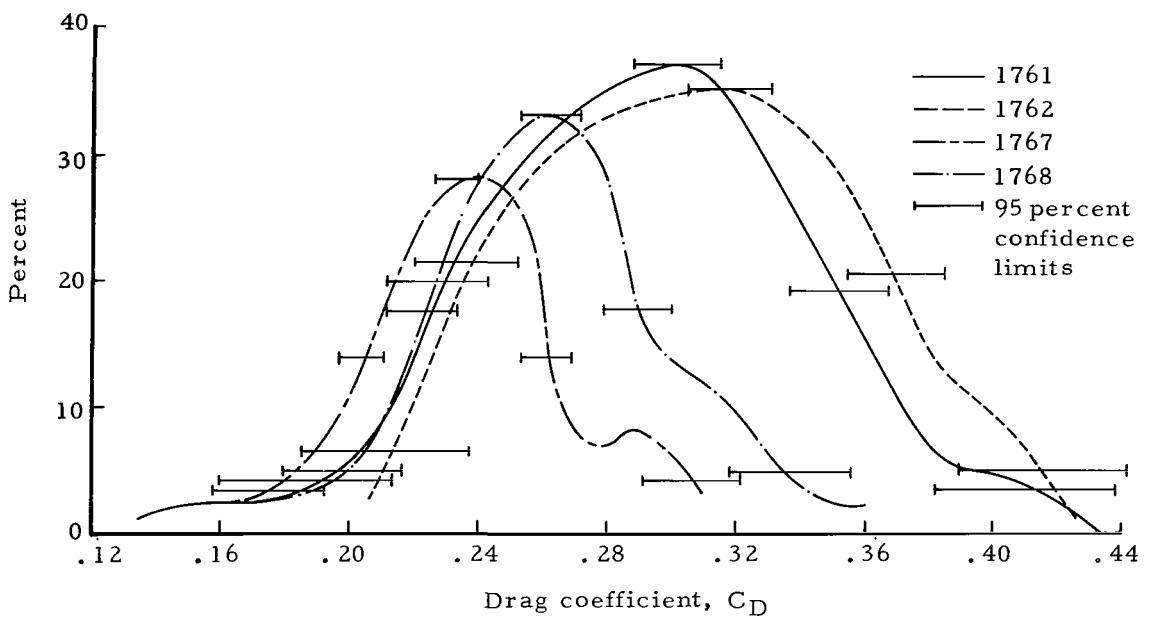

FIGURE 8. PROBABILITY DISTRIBUTIONS OF THE DRAG COEFFICIENT

coefficient varying between approximately 0.32 for the 2-m (6.56-ft) diameter sphere to 0.24 for the 2.13- and 2.44-m (7- and 8-ft) diameter spheres. This variation in average drag is caused by variation in balloon size and ascent rate. Average values of the drag coefficient for a 2-m (6.56-ft) diameter sphere calculated by Scoggins [16] agree very closely with the most probable value of 0.32 obtained above for supercritical flow. The most probable values for the other spheres are about a factor of 2 larger than those determined in wind tunnels [3].

Spectra of the drag force and the drag coefficient are shown in Figures 9 and 10. Spectra of the drag force do not show any preferred periods of oscillation except at low Strouhal numbers, a fact which is caused by a large steady-state

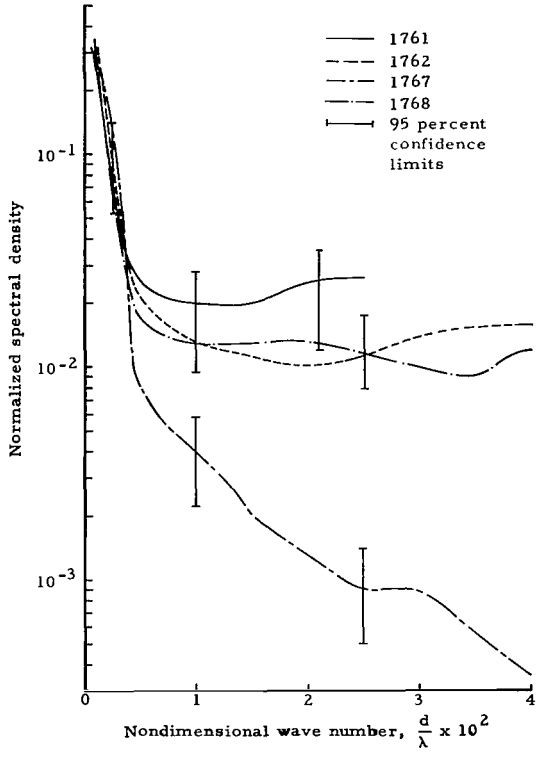

FIGURE 9. SPECTRA OF DRAG FORCES

value. In the case of an ascending balloon, the Strouhal number is given by the ratio of balloon diameter to the vertical wave length, $\frac{d}{\lambda}$. This is a nondimensional wave number which is independent of the ascent rate of the balloon. For all tests except 1767, nondimensional wave numbers above 0.01 contain about equal energy. This means that oscillations in drag over small ascent distances occur randomly. Spectra of the drag coefficients for the larger balloons (tests 1767 and 1768) show peaks near nondimensional wave numbers of 0.013 and 0.030. The overall trend in all spectra is a decrease in energy with an increase in nondimensional wave number.

According to Blackman and Tukey [32], the accuracy or statistical confidence of a computed spectral estimate depends upon the length of record and the number of lags used. Spectral estimates are considered as a chi-square variate with the number of degrees of freedom, k, given approximately by $2T_n/T_m$, where T_n is the length of record and T_m is the maximum lag. In the spectrum analysis which follows, the number of degrees of freedom is approximately 15. According to Blackman and Tukey, the computed spectral estimates for 15 degrees of freedom will be within approximately ± 50 percent of their value with 95 percent confidence. These confidence limits are shown on all spectra.

Lift. Probability distributions of lift in the y-direction are shown in Figure 11. Distributions in the x-direction were similar to those in the y-direction. Magnitudes of the lift forces in all directions increase with balloon size with the magnitude in the z-direction being several times smaller than in the x- and y-directions. This is caused by the orientation of the wake. The z-component of lift is always negative because of the large force of buoyancy which causes a large composite force, F_z, in the negative z-direction, which, in turn, determines

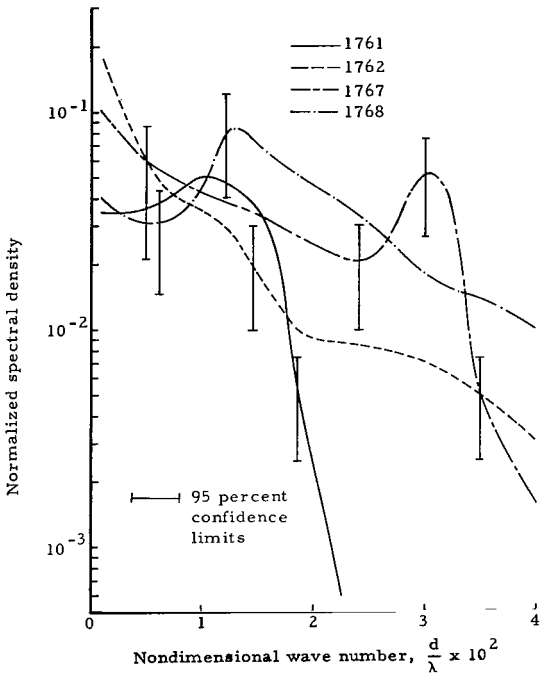

FIGURE 10. SPECTRA OF DRAG COEFFICIENTS

the sign of F_z. Probability distributions of lift in the z-direction are shown in Figure 12. For all balloons, the magnitudes of the component lift forces in the x- and y-directions are almost symmetrical about zero and have the same distribution in both directions, indicating no statistical preference for direction.

Probability distributions of the magnitude of the lift vector are shown in Figure 13. Distributions of the horizontal component of lift were very similar to those of the total lift force indicating that the lift force is predominantly horizontal. The average magnitude of the lift force increases with balloon diameter.

Distributions of the lift coefficient defined by equation (29) are shown in Figure 14. The most frequently occurring value varies between approximately 0.03

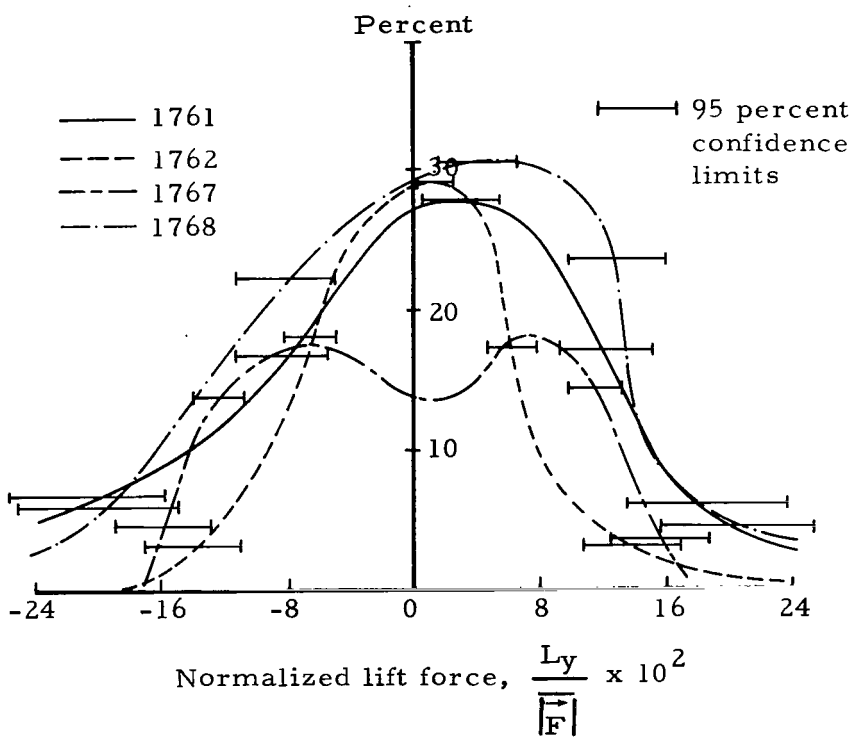

FIGURE 11. PROBABILITY DISTRIBUTIONS OF NORMALIZED LIFT ALONG y-AXIS

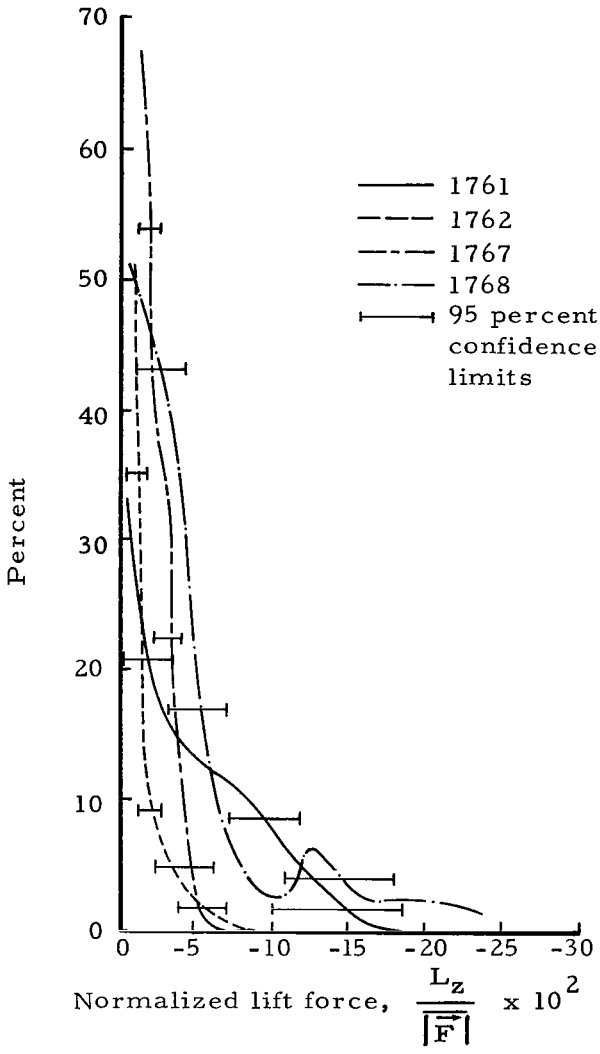

FIGURE 12. PROBABILITY DISTRIBUTIONS OF NORMALIZED LIFT ALONG z-AXIS

and 0.05; however, the distributions for tests 1761 and 1768 are flat with a relatively high percentage of occurrences of coefficients as large as 0.07.

Curves of the mean and RMS values of the lift coefficient versus Reynolds number in the supercritical range are shown in Figure 15. The mean and RMS values of the lift coefficients, which differ very little in magnitude, decrease with an increase in Reynolds number. Fung [11] obtained a similar relationship for circular cylinders at Reynolds numbers below approximately 4×10^5 (see Figure 1). The curves in Figure 15 have been extended to lower Reynolds numbers to indicate the sharp decrease in the lift coefficient which occurs at subcritical Reynolds numbers.

Spectra of the total lift force are shown in Figure 16. Spectra of the horizontal lift force were almost identical to those of the total lift force. Spectra of the total lift force show relatively constant energy at nondimensional wave numbers above 0.01, but do show a tendency toward increased energy at lower nondimensional wave numbers. This indicates that changes in the lift force at lower nondimensional wave numbers are somewhat more organized than at higher nondimensional wave numbers. Stated differently, the lift force experiences somewhat organized large-scale variations with superimposed random variations. Spectra of the horizontal lift force show the same features indicating the lift force is primarily horizontal.

Spectra of the lift coefficient are given in Figure 17. Low energy is shown for tests 1762 and 1767 at nondimensional wave numbers of 0.013 and 0.035, respectively, with an overall decrease in energy with an increase in nondimensional wave number.

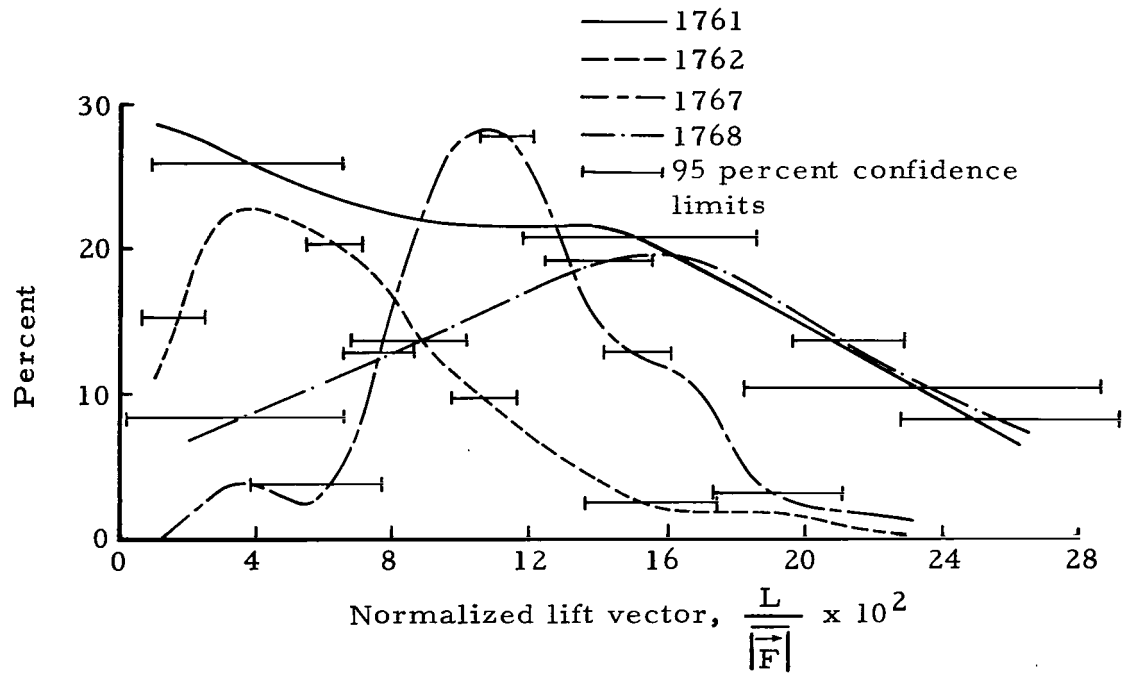

FIGURE 13. PROBABILITY DISTRIBUTIONS OF THE MAGNITUDE OF THE NORMALIZED LIFT VECTOR

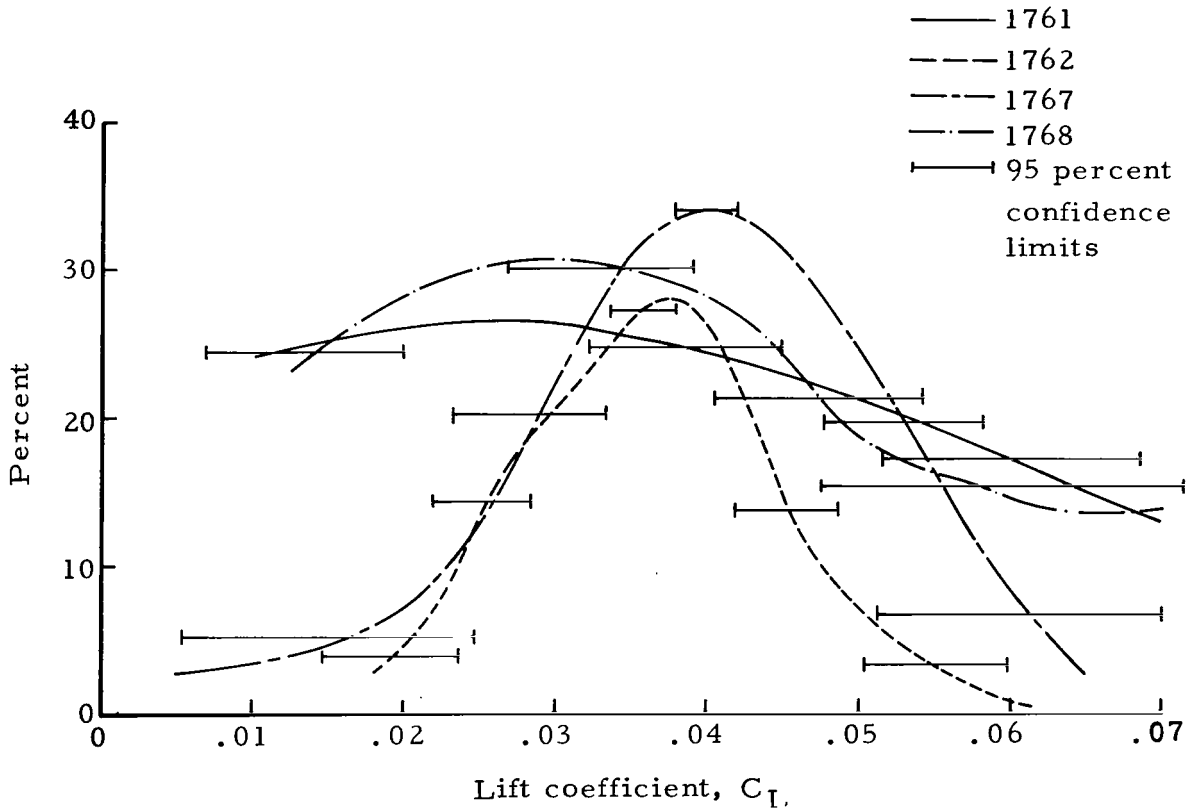

FIGURE 14. PROBABILITY DISTRIBUTIONS OF THE LIFT COEFFICIENTS

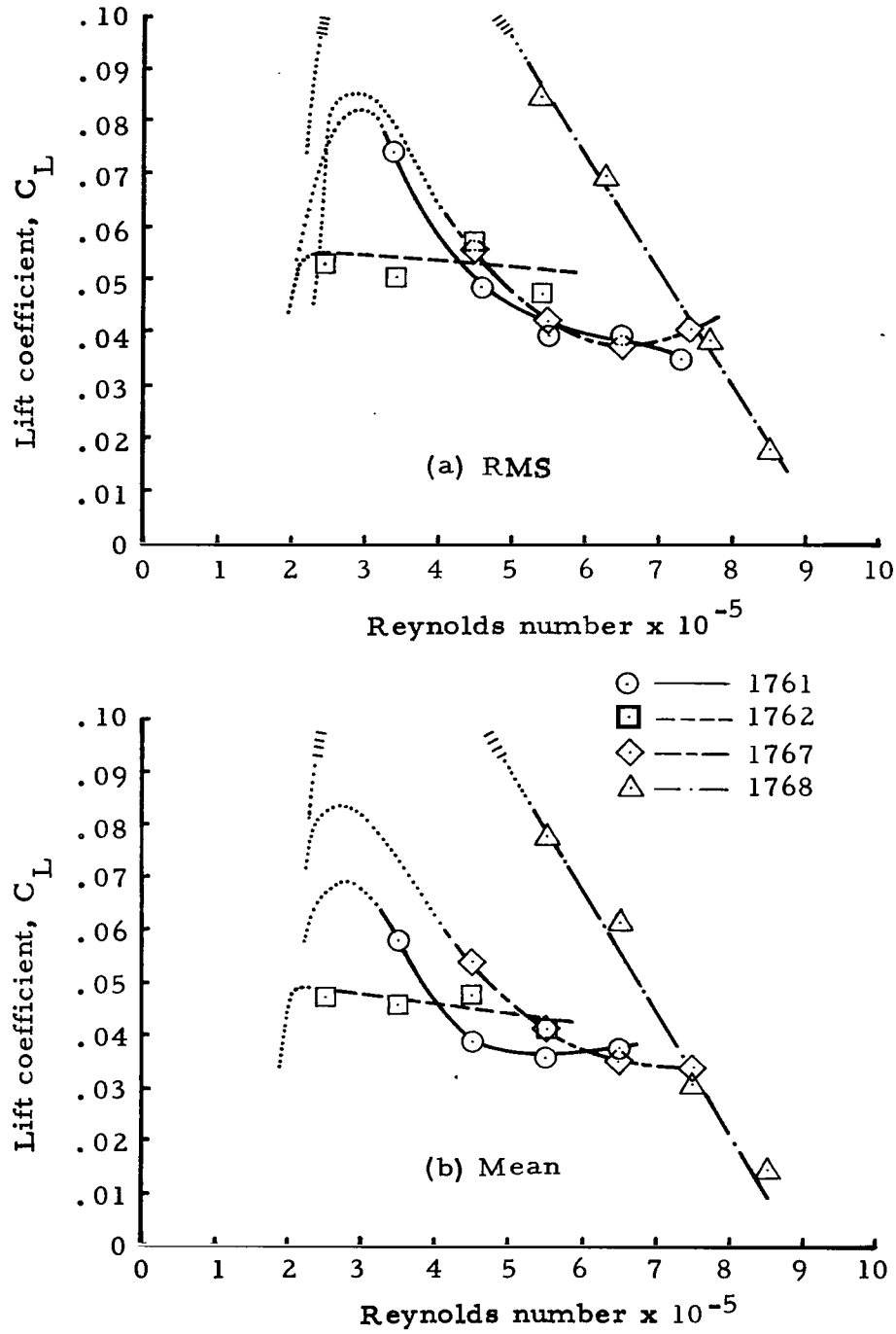

FIGURE 15. MEAN AND RMS VALUES OF THE LIFT COEFFICIENT

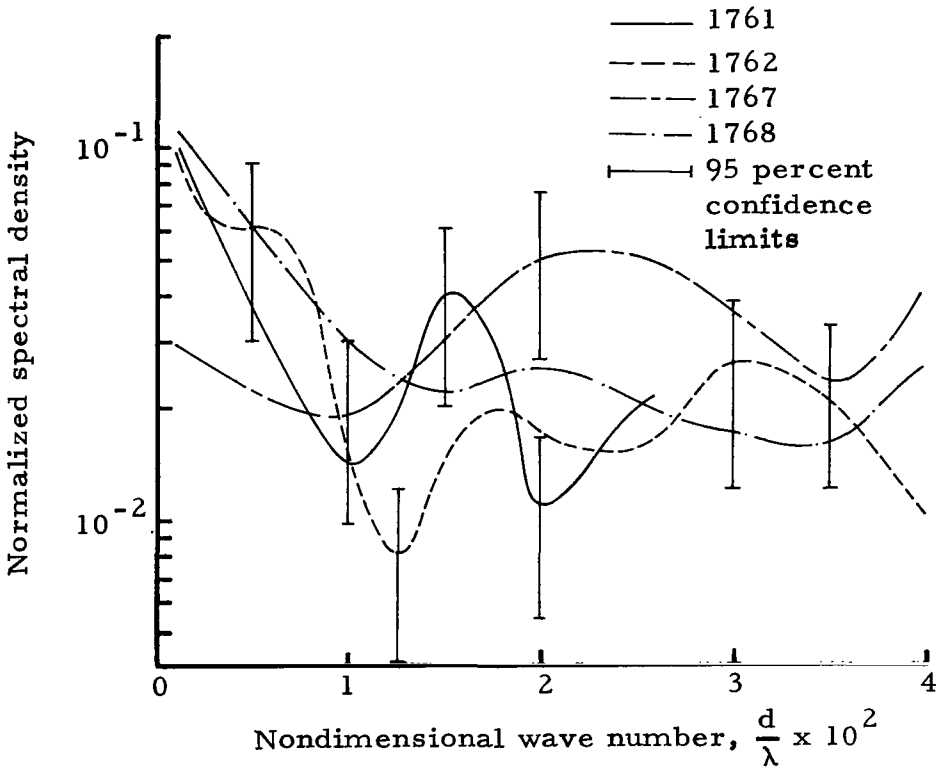

FIGURE 16. SPECTRA OF TOTAL LIFT FORCES

Spectra of the changes in direction of the horizontal lift force defined by equation (27) are shown in Figure 18. With the exception of test 1767, which has a peak near a nondimensional wave number of 0.030, the only significant feature of these spectra is an overall increase in energy with an increase in nondimensional wave number. This means that short period changes in the direction of the horizontal lift force occur with more regularity than the longer period changes.

Relationship Between Total and Drag Forces

It was assumed previously that the drag vector acted in the direction of the relative velocity vector, but there was no restriction placed on the direction of the total force vector. The angle between these two vectors is a function of the magnitude and direction of the lift force. Only a small percentage of the angles is greater than 16 degrees (cosine α = 0.97), with the percentage increasing sharply for the smaller angles. These large angles are indicative of an unstable balloon and are caused by large lift forces.

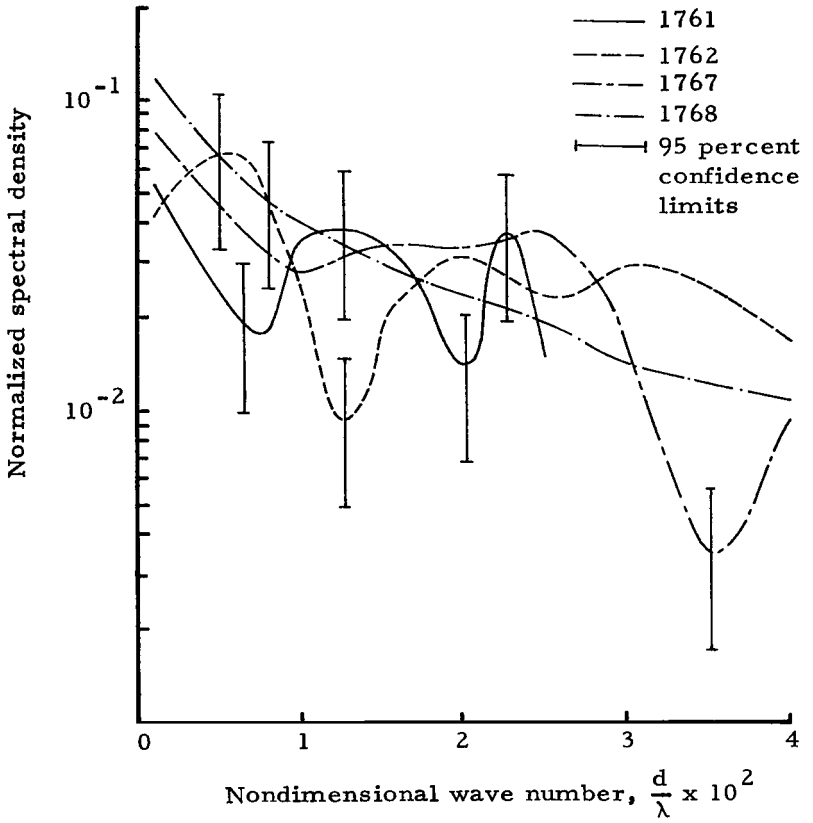

FIGURE 17. SPECTRA OF LIFT COEFFICIENTS

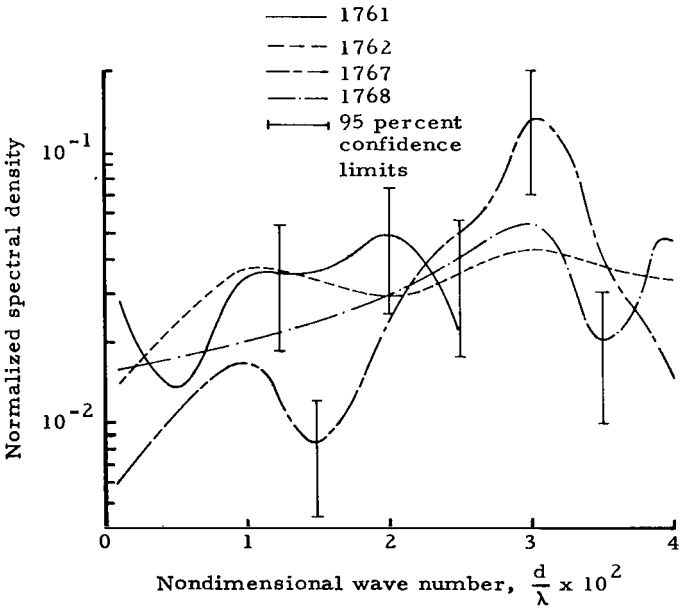

FIGURE 18. SPECTRA OF CHANGES IN HORIZONTAL DIRECTION OF LIFT FORCES

THE EXPERIMENTAL DESIGN OF AN ACCURATE SPHERICAL BALLOON WIND SENSOR

Based on work done by Killen [1], Scoggins [15, 16], MacCready and Jex [13] and Rogers [17], it became apparent that the instability of a sphere moving through a fluid is associated with an unstable wake causing erratic lift and drag forces. Also, it is evident from the results presented in the preceding section that a smooth, superpressure balloon large enough to reach a 20-km altitude is not a satisfactory wind sensor for the troposphere (surface to 12 km). Elimination of the lift forces is required in order to stabilize the wake. Although much has been learned about the aerodynamic behavior of such balloons, a complete understanding still does not exist, and it is not possible to describe analytically the spurious motions observed when the balloon rises through the atmosphere. Even if an exact analytical description were available, the interaction between the wind field and the balloon would have to be known before accurate wind measurements could be made. This would require a prior knowledge of the wind field which is the very thing we desire to measure.

With this background an approach was taken, based on present knowledge and sound theoretical principles, to conduct an experimental program aimed at developing an accurate spherical balloon wind sensor. The problem appears to be that of controlling vortex formation and separation which, in turn, controls lift and drag. To do this, balloons with varying types of roughness elements were fabricated and flown, and the data were analyzed to determine what influence the roughness elements had on the spurious motions. Roughness elements change the velocity profile in the boundary layer which causes earlier separation as in the case of a subcritical sphere. Based on results obtained from each series of tests, additional configurations were flown and data analyzed. The process was repeated until the desired results were obtained. Eight configurations were tested.

Wind profiles were measured by the smoke trail method [23] and used as a reference in evaluating the effectiveness of roughness elements to eliminate spurious motions. An experimental analysis (Appendix B) shows that the smoke trail wind data has an RMS error of generally less than 0.5 m/sec.

In addition to smoke trail wind profile data, the 1.22-m (4-ft) diameter, smooth, superpressure balloon was also used as a reference in each series. Even though this balloon experiences self-induced motions [17, 33, 34], it can be used as an indicator of performance when operating in the subcritical flow regime for comparison with other balloons. The 1.22-m (4-ft) diameter sphere

goes from supercritical to subcritical Reynolds numbers at an altitude of approximately 4 to 6 km. Below this altitude the balloon operates in the supercritical Reynolds number regime and is unstable. An appreciation for the difference in a balloon operating at subcritical Reynolds numbers and at supercritical Reynolds numbers may be gained by comparing the spectra for the 1.22-m (4-ft) diameter balloon below the transition altitude with that above. For example, spectra of the small-scale scalar balloon motions (see subsection following, "Analysis of Measured Balloon Motions," for definition) are shown in Figure 19 between 2.5 and 6 km (supercritical) and between 6 and 13.3 km (subcritical).

In the development of an improved wind sensor, emphasis must be placed on the characteristics of the measured small-scale motions. In this section the effects of various sizes and shapes of roughness elements on the variability and spectra of small-scale motions are presented. The effects of roughness elements and attitude orientation on aerodynamic stability are discussed. Drag curves for various balloon configurations and a comparison of smoke trail and balloon-measured wind profile data are also discussed.

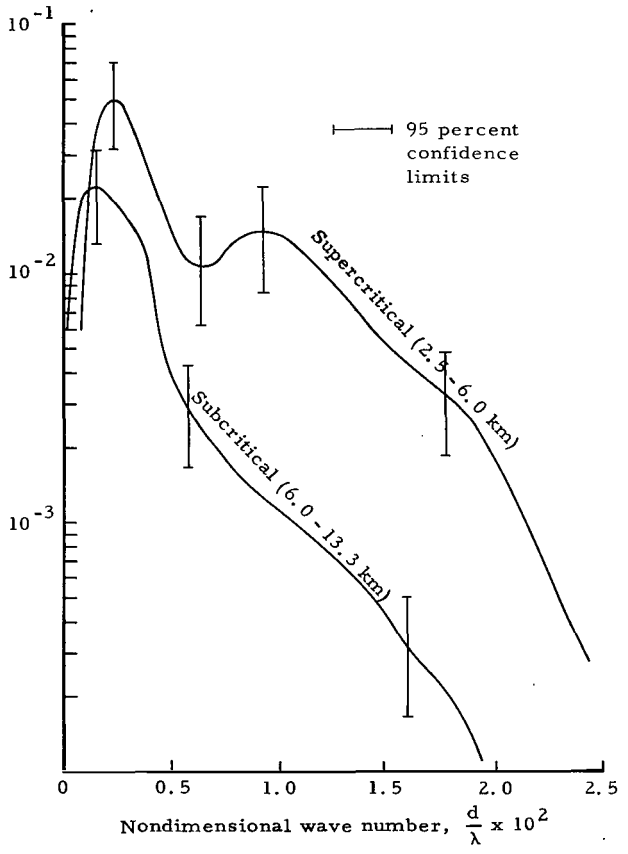

FIGURE 19. SPECTRA OF SMALL-SCALE SCALAR MOTIONS FOR SAME BALLOON IN SUB- AND SUPERCRITICAL FLOW REGIMES

The Experimental Program

The experimental program consisted of flying spheres of different configurations in sequence on the same day. The types of balloons were alternated to provide comparisons between as many balloon configurations as possible. The test series were conducted when the radar was available rather than during chosen weather conditions. It turned out that low wind speeds existed during all the test series. All balloons were launched from the same location and tracked by the same radar. Pre- and post-calibrations of the radar were accomplished.

Data for three series of balloon flights are shown in Table I. A number of additional series similar to these were also flown. Table I is self-explanatory except for the column headed "type." This column refers to the configuration; e.g., 2m, 3T(*or* F), 9S refers to a balloon 2 m in diameter (2m) with 3-inch (0.076-m) high truncated or full cones (3T or F) spaced 9 inches (0.2286 m) apart on the sphere (9S). The "weight" column refers to the balloon alone and does not include the gas.

TABLE I. DATA FOR SERIAL BALLOON FLIGHTS

Test Number	Release Time (Z)	Type*	Weight (g)
	Series 1 - June 9, 1964		
4378	1800	4 ft smooth	163
4379	1916	2m, 3T, 9S	301
4380	2045	2m, 3F, 7S	301
4381	2210	4 ft smooth	164
4382	2345	2m, 4F, 7S	310
4383	0115	2m, 3T, 9S	308
4387	1900	Smoke trail	
	Series 2 - June 11, 1964		
4384	1400	4 ft smooth	163
4385	1521	2m, 3F, 7.5S	302
4386	1640	2m, 4F, 8S	308
4393	1806	4 ft smooth	165
	Series 3 - June 12 and 13, 1964		
4405	1700	4 ft smooth	164
4497	1830	2m, 2T, 6S	400
4498	1950	2m, 2T, 6S	300
4499	2245	4 ft smooth	164
4500	0016	2m, 2T, 6S	600
4502	0130	2m, 2T, 6S	1000
4503	1900	Smoke trail	

* These units have not been converted to S.I. units.

Analysis of Measured Balloon Motions

Definition of Small-Scale Motions. Since the problem is to develop a wind sensor that will respond accurately to small-scale changes in the wind field, emphasis must be placed on analyzing the higher frequency components of the measured profiles. For this section small-scale motions are defined as those which are not included in the rawinsonde measured profiles. This definition is not of too much importance as long as the longer wavelengths included in the definition of small-scale motions are longer than the longest wavelength of the self-induced motions. With this definition, wavelengths as long as approximately 500 m are included, extending well beyond the wavelengths of all spurious balloon motions.

The small-scale components of motion were separated from the profiles by defining a filter function by the relationship

$$S_R(f) = |F|^2 S_S(f) \tag{30}$$

where S_S is the spectrum of the wind profile measured by the smoke trail method and assumed to be the true wind speeds, S_R is the spectrum of the wind profile measured by the rawinsonde system, and F is the filter function. The filter function, and the weights which must be applied at 50-m intervals to a detailed (25-m interval) profile in order to produce a smooth profile containing the same frequency content as would have been measured by the rawinsonde system, is shown in Figure 20. The weights were obtained by taking the cosine transform of the filter function, then normalizing. The small-scale motions (wavelengths less than approximately 500 m) are obtained by applying the filter weights in a step-wise manner to a detailed wind profile to define a smooth profile, then subtracting this smooth profile from the detailed profile. The higher frequency motions represented by the difference between the smoothed and detailed profiles are used to assess the stability of the various balloons. Equation (30), with smoke trail data replacing rawinsonde data and balloon data replacing smoke trail data, was used to define erratic balloon motions used in the preceding section.

The resulting filter function was similar to that shown in Figure 20 but with a cutoff near a wavelength of 300 m. The same weights are used but applied

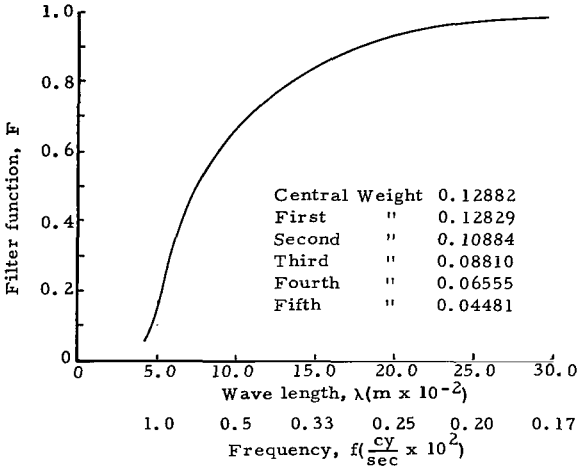

FIGURE 20. FILTER FUNCTION USED FOR DEFINING SMALL-SCALE MOTIONS

at 25-m intervals rather than 50-m intervals.

General Observed Features from Serial Ascents. Profiles of balloon motions for the test series presented in Table I will not be shown here. Most of the profiles exhibited features somewhat similar to those shown in the preceding section but with much less spurious motions. The profiles measured with the rough balloon configurations show variable scatter over limited altitude bands, although the scatter was in most cases not sufficient for detection when plotted. For this reason it was necessary to use quantitative methods in assessing performance of the balloons. Remarkable consistency was noted between adjacent profiles indicating that true larger scales of the wind motions were being measured.

Performance of the Various Balloon Configurations. The performance of each balloon was evaluated by computing the variance and spectra of the small-scale motions for each flight and comparing with data obtained with the 1.22-m (4-ft) diameter sphere and smoke trail. The energy or variance associated with each test shown in Table I and the altitudes over which each spectrum was computed, are shown in Table II. Variations in the amount of energy contained in the small-scale motions from one profile to another are clearly shown in Table II.

The variances associated with each profile using the rough balloon configurations were generally larger than those for the 1.22-m (4-ft) diameter smooth balloon in the subcritical Reynolds number flow regime and for the smoke trail profiles. From visual observations of the ascent of several of the balloons, it was noted that they were experiencing some rotation. It was further observed that when rotations occurred the balloon appeared to experience somewhat larger lateral motions. The roughness elements had eliminated a large percentage of the spurious motions by forcing flow separation and reducing lift, but the rotation apparently produced a small lift force which still had to be eliminated. This was done by attaching a small mass at a point on the sphere which displaced the center of gravity downward, thus providing a stabilizing torque. This also increased the density ratio which has a stabilizing effect [12]. Spectra for Jimsphere type

TABLE II. VARIANCE AND ALTITUDE DATA CORRESPONDING TO BALLOON FLIGHTS PRESENTED IN TABLE I

Test Number	Altitude Range (km)	Variances Zonal (V_x)	Variances Meridional (V_y)	Variances Scalar ($\|V\|$)
	Series 1 - June 9, 1964			
4378	3.0 - 14.0	0.246*	0.211*	0.211*
4379	2.0 - 20.0	0.432	0.435	0.381
4380	3.5 - 20.0	0.431	0.442	0.340
4381	2.0 - 8.0	0.634	0.715	0.732
	8.0 - 15.0	0.159	0.246	0.106
4382	8.0 - 15.0	0.208	0.289	0.210
	3.5 - 20.0	0.494	0.601	0.541
4383	2.0 - 20.0	0.489	0.587	0.457
	Series 2 - June 11, 1964			
4384	2.0 - 6.0	0.576	0.462	0.522
	6.0 - 13.3	0.095	0.186	0.145
4385	2.0 - 16.0	0.514	0.419	0.594
4386	3.0 - 18.0	0.450	0.452	0.452
4393	1.8 - 5.5	0.420	0.682	0.334
	6.5 - 14.0	0.173	0.178	0.144
	Series 3 - June 12 and 13, 1964			
4405	5.0 - 10.0	0.517	0.482	0.502
4497	6.0 - 14.0	0.162	0.204	0.226
4498	6.0 - 14.0	0.204	0.243	0.226
4499	2.5 - 7.0	0.366	0.531	0.378
	7.0 - 14.0	0.217	0.254	0.134
4500	2.5 - 15.0	0.185	0.193	0.184
4502	3.5 - 13.0	0.161	0.160	0.158

* m^2/sec^2

2m, 3F, 7.5S with a 100-g mass attached, smoke trail, and a 1.22-m (4-ft) diameter sphere operating at subcritical Reynolds numbers were almost identical. This means that RMS errors caused by erratic motions associated with Jimsphere balloon type 2m, 3F, 7.5S with a mass of 100 g attached are no larger than those associated with the smoke trail and 1.22-m (4-ft) diameter sphere data. As noted by Rogers and Camitz [17] this Jimsphere configuration experiences a regular spiral motion with a wavelength near 25 m. This spiral motion is eliminated by the data reduction method presented in Appendix A [17].

Drag Coefficient Curves

The value of the drag coefficient is of primary interest in computing the response of a balloon to a change in wind. The magnitude of the drag force, which accelerates the balloon in the presence of a wind shear, is directly proportional to the magnitude of the drag coefficient. Thus large drag coefficients are desirable.

The magnitude of the drag coefficient increases with the size of the wake. The drag coefficient measured in wind tunnels for smooth spheres is small at supercritical Reynolds numbers where the wake is small, increases sharply in the transition range, and has a much larger and almost constant value at subcritical Reynolds numbers where the wake is large [3, 4]. A minimum is observed at supercritical Reynolds numbers immediately above the transition range. The addition of roughness elements to a spherical balloon causes separation near the equator, resulting in a large wake and a large drag coefficient at all Reynolds numbers.

Drag coefficient curves are shown in Figure 21 for Jimsphere type 2m, 3F, 7.5S calculated from full-scale flight data and measured in a wind tunnel using a scaled model. For comparison, a curve measured in a wind tunnel using a smooth sphere is also shown. The drag coefficient calculated from full-scale data is larger at all Reynolds numbers than was determined in the wind tunnel.

Preukschat [12] found that the ratio of the density of a sphere to the density of the fluid was an important factor in determining how the sphere will move through the fluid. A sphere constrained in a wind tunnel has an effective infinite density, while a sphere such as type 2m, 3F, 7.5S rising in the atmosphere has an average density ratio of about 0.4. This difference in density ratios may account, at least in part, for the difference in the drag coefficient curves. Another factor which may account for some of the difference is that a free-rising

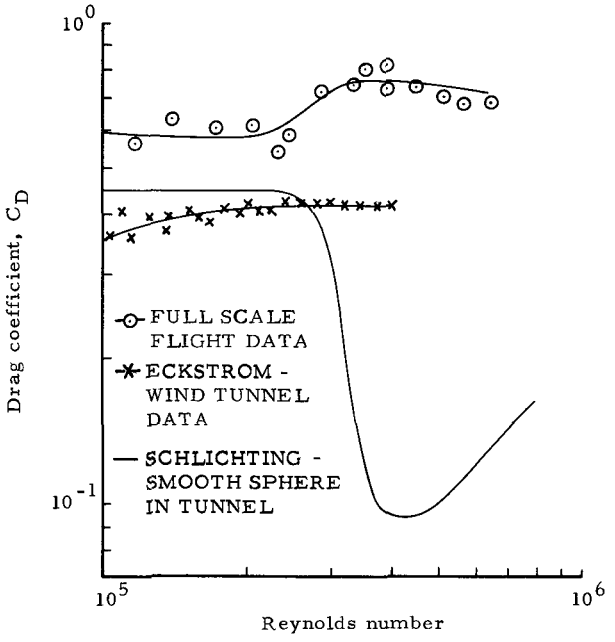

FIGURE 21. DRAG COEFFICIENT CURVES FOR JIMSPHERE TYPE 2m, 3F, 7.5S AND FOR A SMOOTH SPHERE IN A WIND TUNNEL

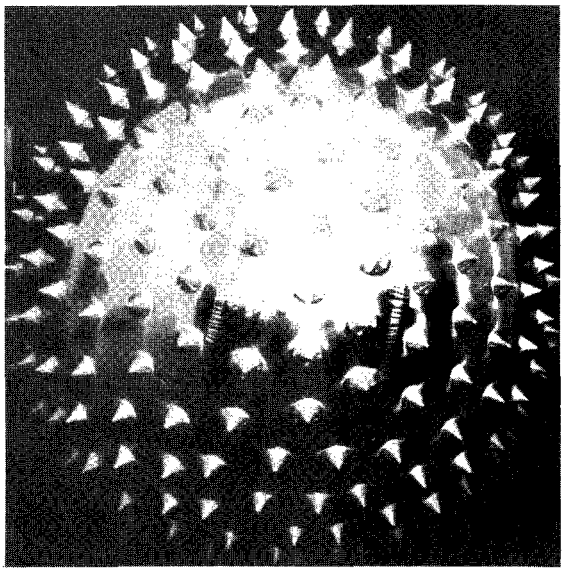

FIGURE 22. JIMSPHERE TYPE 2m, 3F, 7.5S

balloon can adjust very quickly to changes in forces caused by a nonsymmetrical or tilted wake, thus keeping the drag vector pointing opposite the direction of motion of the balloon. Scoggins [16] investigated the drag coefficient for a rough balloon with a density ratio of about 0.8, and computed a drag curve almost identical to the curve determined in a wind tunnel with a model of type 2m, 3F, 7.5S (Fig. 21). This supports the hypothesis that the difference in the curves in Figure 21 for the rough spheres is accounted for, at least in part, by the difference in density ratios.

Dynamic Response Characteristics of Aerodynamically Stable Rough Balloons to Vertical Wind Shears

Eckstrom [20], using the drag coefficient curve determined in wind tunnel tests and presented in Figure 21, investigated theoretically the response of Jimsphere type 2m, 3F, 7.5S to wind shears. This balloon is shown in Figure 22. Eckstrom found that the Jimsphere would respond with a lag of less than 1 m/sec to the maximum expected wind shear of 0.2 sec^{-1} at all altitudes below 13 km. Below 10 km the lag is less than 0.3 m/sec. Using the drag curve determined from full-scale flight data, these lag errors would be even less. In either case, the balloon responds rapidly enough to permit the measurement of wind shears over a few balloon diameters. In practice, when radar tracking errors and data reduction are considered, average winds over 25 to 50 m can be measured with an RMS error of generally less than 0.5 m/sec.

A typical scalar wind speed profile measured with the Jimsphere is shown in Figure 23. Spurious balloon motions associated with smooth, superpressure balloons of the same size as the Jimsphere, and shown in Figure 3, have been eliminated. The same data reduction method was used in both cases.

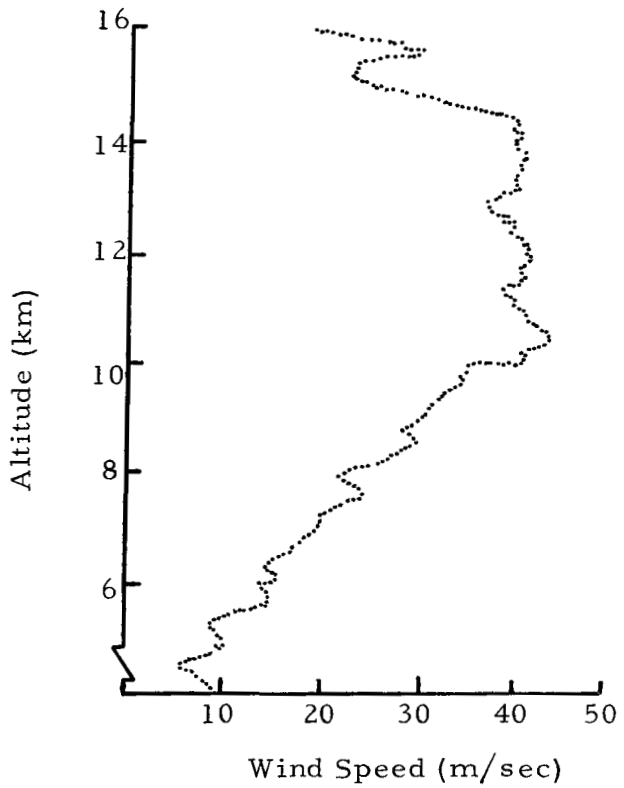

FIGURE 23. SCALAR WIND SPEED PROFILE MEASURED WITH JIMSPHERE

CONCLUSIONS

The following specific results were obtained in this study:

1. The statistical properties of spurious motions associated with smooth, superpressure, spherical balloons operating at supercritical Reynolds numbers are predictable.

2. There were no systematic differences observed in the spurious motions associated with balloons of 1.22 m (4 ft), 2 m (6.56 ft), 2.13 m (7 ft), and 2.44 m (8 ft) in diameter.

3. Composite, lift, and drag forces along the horizontal axes are nearly symmetrical with a mean near zero.

4. Spurious balloon motions in the x-z and y-z planes occur with equal magnitude and frequency, and have a mean in each plane of near zero.

5. Distributions of the drag coefficients for balloons of various diameters are nearly symmetrical with the average value varying between 0.30 for the 1.22-m (4-ft) diameter sphere to 0.25 for 2.13-m (7-ft) and 2.44-m (8-ft) diameter spheres.

6. The drag force does not contain any preferred periods of oscillations.

7. The lift force is predominantly horizontal.

8. Magnitudes of the component lift forces in the x and y directions are almost symmetrical with a mean near zero.

9. Magnitudes of the component lift forces increase with balloon size with the magnitude in the z-direction being several times smaller than in the x- and y-directions.

10. The most frequently occurring values of the lift coefficient vary between 0.03 and 0.05 with the value reaching as high as 0.07 ten percent or more of the time.

11. Mean and RMS values of the lift coefficient decrease with an increase in Reynolds number in the supercritical range.

12. The lift force experiences somewhat organized large-scale variations with superimposed random variations. While there are no preferred modes of variation, there is a tendency toward organized variations at nondimensional wave numbers below 0.013.

13. Assuming that changes in direction of the horizontal component of lift are indicative of vortex formation and separation, there are no preferred periods for these events; however, the shorter period changes occur with more regularity than the longer period changes.

14. The angle between the total force and drag vectors usually does not exceed 15 degrees.

15. The addition of conical roughness elements 0.076 m (3 in.) in height, 0.076 m (3 in.) in base diameter, and spaced 0.19 m (7.5 in.) apart, and a point mass of 100 g to a spherical balloon produces stabilization and essentially eliminated spurious motions. The roughness elements produce more and smaller vortices than those associated with smooth balloons. The superposition of the smaller vortices onto the larger ones produces an equal distribution of energy in the lift forces over all frequencies.

16. Damping and inertia of the rough balloon (Jimsphere) with a point mass of 100 g attached prevent significant rotation and thus eliminate lift at higher nondimensional wave numbers.

17. The maximum expected wind shear of 0.2 sec^{-1} is small compared with V_z/d, where V_z is the ascent rate of the Jimsphere and d its diameter; therefore, wind shear would not significantly affect the balloon's response capabilities.

18. The drag coefficient for the rough balloon is almost independent of Reynolds number and has a large value at all altitudes.

19. Jimsphere type 2m, 3F, 7.5S with a mass of 100 g attached provides wind profile measurements averaged over 25- to 50-m altitude intervals with an RMS accuracy of about 0.5 m/sec or less to an altitude of 18 km when tracked by the FPS-16 radar.

Suggestions for Further Research

Although this investigation has provided much information on sphere behavior and the forces producing this behavior in the supercritical Reynolds number flow regime, there are still several fundamental problems to be solved. Of particular interest are the phenomena of the formation and separation of individual vortices, more explicit relationships between drag, lift, buoyancy, and apparent mass effects, the influence of extreme wind shears and turbulence on the response of a sphere, and the influence of the wake on the motions of the sphere. Further research is also desired in developing a fast-rising wind sensor that can reach 18 km within a few minutes (or a system which will otherwise measure a vertical wind profile in a short time) rather than the 1 hour required by the present configuration. Finally, data handling procedures need refining to improve the quality of the measured wind data.

George C. Marshall Space Flight Center
National Aeronautics and Space Administration
Huntsville, Alabama, March 6, 1967
160-44-04-00-62

APPENDIX A

DATA REDUCTION PROCEDURE FOR SUPERPRESSURE SPHERICAL BALLOONS WITH DISCUSSION ON ACCURACY OF WIND DATA

Edit and Computation Procedure

The processing of radar data to get wind data is a very important function for any system used. Accuracy of the wind data often depends upon the methods employed in processing the basic tracking data which, in turn, are often limited by available computing facilities. The procedure for processing fast rate (0.1-sec interval) tracking data presented here was developed for use on an IBM 7094 computer [19]. While in all probability it is not an optimum program in terms of providing the most accurate wind data possible, it does give satisfactory results for most applications and requires only a nominal amount of computer time. There are essentially two parts to the procedure; one is editing the radar tracking data to eliminate erroneous points, and the other is processing the edited data to get winds. Each of these aspects of the program will be covered separately.

Data Edit Procedure. The data edit procedure is quite simple. The problem is to eliminate values which are not accounted for by trend or random error, and to replace them by values which are reasonable. The first step is to fit the measured values of r, θ, and ϕ (slant range, elevation and azimuth respectively) to a 9-point, first degree equation by the method of least squares. If the residual at the mid-point of the 9-point interval is greater than 3 times the assumed RMS error (provided by the radar manufacturer or obtained by experiment), the point is replaced by the average value over the interval. In order to prevent including stray points in the computation of the mean, the next point immediately following the 9 points used in the curve fit is compared with the 9-point mean, and if the difference is 5 times greater than the assumed RMS error, the point is replaced by the mean. This procedure is repeated for each 0.1-sec step until all the data have been edited.

Wind Computation Procedure. The procedure for computing winds using the edited radar tracking data is given below as a series of steps.

a. Convert slant range from yards to meters, and azimuth and elevation angles from degrees to radians.

b. Compute x, y, and z for each point:

$x = r \cos\theta \cos\left(\phi - \frac{\pi}{2}\right)$ (positive east)

$z = r \sin\theta$ (positive vertical)

$y = r \cos\theta \cos\phi$ (positive north)

c. Correct position coordinates x, y, and z for earth's curvature:

$$x_c = r_o \tan^{-1} \frac{x}{r_o + z}$$

$$z_c = [x^2 + (z + r_o)^2 + y^2]^{\frac{1}{2}} - r_o$$

$$y_c = r_o \tan^{-1} \frac{y}{[x^2 + (z + r_o)^2]^{\frac{1}{2}}}$$

$r_o = 6,373,334$ m = radius of earth at Eastern Test Range, Florida.

d. Determine altitude and corresponding time for 25-m intervals as follows:

1) Find the first z_c which is greater than the desired altitude.

2) Use this z_c as the mid-point of a 41-point (4 sec) least squares first degree curve fit.

3) Determine desired y from polynomial.

4) Repeat 1), 2), and 3) for x_c and y_c.

5) Interpolate linearly between times corresponding to altitudes below and above z to obtain time corresponding to z.

e. Compute component wind speeds $\dot{x}_n$, and $\dot{y}_n$, the scalar wind speed v_n, and vertical velocity of the balloon $\dot{z}_n$, using the following equations:

$$\dot{x}_n = \frac{x_n - x_{n-1}}{\Delta t_{(n,\ n-1)}} \qquad \text{(m/sec)}$$

$$\dot{y}_n = \frac{y_n - y_{n-1}}{\Delta t_{(n,\ n-1)}} \qquad \text{(m/sec)}$$

$$\dot{z}_n = \frac{z_n - z_{n-1}}{\Delta t_{(n,\ n-1)}} \qquad \text{(m/sec)}$$

$$v_n = [\dot{x}_n^2 + \dot{y}_n^2]^{\frac{1}{2}} \qquad \text{(m/sec)}$$

The computed wind speeds are associated with the top of the layer designated by n.

f. Compute direction from which the wind is blowing, Ψ_n, as follows:

$$\Psi_n = \tan^{-1} \frac{\dot{x}_n}{\dot{y}_n} + \text{quadrant correction}$$

The quadrant correction is determined from the sign of $\dot{x}_n$ and $\dot{y}_n$ as follows:

$\dot{x}_n$ +, $\dot{y}_n$ −	$360 - \Psi_n$
$\dot{x}_n$ +, $\dot{y}_n$ +	$\Psi_n + 180$
$\dot{x}_n$ −, $\dot{y}_n$ +	$180 - \Psi_n$
$\dot{x}_n$ −, $\dot{y}_n$ −	Ψ_n.

Accuracy of Computed Wind Data

Error analyses have been conducted for determining the accuracy of wind data obtained by tracking a balloon by the FPS-16 radar. The accuracy is a function of the condition of the radar, the operator's experience, and the data reduction procedure used. A practical approach has been followed here to circumvent difficulties in trying to evaluate the errors contributed from each of these factors. The approach was to track the same balloon with 2 radars simultaneously and independently, and then to compare the computed wind profiles. Three pairs of profiles, one from the Western Test Range (WTR), and two from the Eastern Test Range (ETR) were obtained. A 2-m diameter smooth balloon was used at WTR while the Jimsphere was used at ETR. The smooth balloon operates in the supercritical Reynolds number flow regime to an altitude of approximately 13 km; above this altitude the balloon operates in the subcritical Reynolds number flow regime. At subcritical Reynolds numbers, the balloon is aerodynamically more stable and, presumably, the true atmospheric motions are measured. Thus up to approximately 13 km, the balloon oscillated back and forth in both planes (probably a combination of zigzag and irregular spiral motions), causing the radar to "search."

The RMS errors in the computed balloon motions were determined by assuming that each radar had the same RMS accuracy. Independence is also a necessary assumption, but this is obviously satisfied since the radars operate completely independently. The RMS error, $\sigma_{1,2}$, of the sum or difference of two variables (in this case balloon motion or wind speed) having RMS errors of σ_1 and σ_2 is given by the relation [35]

$$\sigma_{1,2}^2 = \sigma_1^2 + \sigma_2^2 .$$

Assuming that both radars have the same RMS tracking accuracy, the above equation becomes

$$\sigma_R = 0.707\, \sigma_{1,2}$$

where σ_R is the RMS error in balloon motions caused by the tracking accuracy of either radar.

The last equation was used to calculate RMS accuracies of the wind data over 2-km intervals for the three profile measurements. The results are shown

in Tables A-I, A-II, and A-III. The smooth balloon (WTR) was aerodynamically unstable to an altitude of approximately 12 km, while the Jimsphere (ETR) was aerodynamically stable at all altitudes. Thus, below approximately 12 km the "search" of the radars is more pronounced in the WTR case than in the ETR cases.

As shown in Table A-I the accuracy of the radars used at WTR improved with altitude and is a factor of 2 to 3 times better between 13 and 20 km than between 2 and 4 km. In contrast, as shown in Tables A-II and A-III, there is only a factor of 1 to 2 improvement in the accuracy of the radars used at ETR for the same altitudes when tracking the aerodynamically stable Jimsphere. This improvement in accuracy is apparently caused by a decrease in spurious motions which causes less searching. At altitudes above 12 km, where both balloons are aerodynamically stable, no significant differences were observed.

TABLE A-I. AVERAGE VALUES OF RADAR COORDINATES AND RMS ERRORS IN WIND DATA AS FUNCTION OF ALTITUDE FOR WTR TEST 3002, 1730Z, MARCH 16, 1963

ALTITUDE INTERVALS (m)	RMS ERRORS				AVERAGE VALUES		
	V_x (m/sec)	V_y (m/sec)	V (m/sec)	V_z (m/sec)	$\overline{\phi}$ (deg)	$\overline{\theta}$ (deg)	$\overline{r}$ (m)
2000 - 3975	0.49	0.66	0.57	0.18	89.4	32.4	6100
4000 - 5975	0.40	0.71	0.49	0.15	79.6	25.0	12,900
6000 - 7975	0.40	0.35	0.40	0.14	75.2	20.4	21,800
8000 - 9975	0.29	0.28	0.27	0.17	73.5	18.4	31,000
10,000 - 11,975	*	*	*	*	*	*	*
12,000 - 13,975	0.23	0.24	0.24	0.23	74.2	15.3	53,200
14,000 - 15,975	0.24	0.18	0.24	0.29	73.6	14.1	65,300
16,000 - 17,975	0.16	0.23	0.17	0.26	73.2	12.9	80,900

* No Data

TABLE A-II. AVERAGE VALUES OF RADAR COORDINATES AND RMS ERRORS IN WIND DATA AS FUNCTION OF ALTITUDE FOR ETR TEST 8920, 1402Z, DECEMBER 23, 1964

ALTITUDE INTERVALS (m)	RMS ERRORS				AVERAGE VALUES		
	V_x (m/sec)	V_y (m/sec)	V (m/sec)	V_z (m/sec)	$\overline{\phi}$ (deg)	$\overline{\theta}$ (deg)	$\overline{r}$ (m)
2000 - 3975	0.30	0.39	0.39	0.32	113.0	30.0	6450
4000 - 5975	0.23	0.16	0.25	0.12	108.0	27.3	11,750
6000 - 7975	0.19	0.19	0.23	0.12	114.7	25.0	17,950
8000 - 9975	0.18	0.28	0.30	0.11	121.9	23.7	24,475
10,000 - 11,975	0.19	0.18	0.22	0.12	130.6	21.7	32,400
12,000 - 13,975	0.27	0.18	0.32	0.13	129.0	18.9	43,500
14,000 - 15,975	0.32	0.18	0.32	0.15	125.1	17.0	55,300
16,000 - 17,975	0.21	0.17	0.24	0.23	123.4	16.3	65,100

TABLE A-III. AVERAGE VALUES OF RADAR COORDINATES* AND RMS ERRORS IN WIND DATA AS FUNCTION OF ALTITUDE FOR ETR TEST 8940, 1600Z, DECEMBER 23, 1964

ALTITUDE INTERVALS (m)	RMS ERRORS			
	V_x (m/sec)	V_y (m/sec)	V (m/sec)	V_z (m/sec)
2000 - 3975	0.30	0.23	0.26	0.17
4000 - 5975	0.16	0.10	0.21	0.14
6000 - 7975	0.17	0.19	0.22	0.13
8000 - 9975	0.23	0.27	0.33	0.20
10,000 - 11,975	0.16	0.19	0.21	0.13
12,000 - 13,975	0.25	0.17	0.27	0.15
14,000 - 15,975	0.28	0.14	0.27	0.19
16,000 - 17,975	0.20	0.18	0.20	0.18

* As shown in Table A-II

APPENDIX B

ACCURACY OF SMOKE TRAIL WIND DATA

Wind data are obtained by the smoke trail method by establishing a vertical column of smoke using a small rocket, then determining movement of the smoke trail photographically in time. The smoke trail is assumed to move with the speed of the wind.

Analytical procedures for computing wind speeds (horizontal displacement of the smoke trail during some convenient time period) are presented by Houston [36] and Foster [37]. These procedures are not difficult mathematically, but it is difficult to establish analytically the accuracy of the computed wind data because of the subjectivity involved. For example, locating the center of the trail is a matter of judgement. Errors in wind data are also caused by film shrinkage, survey errors, camera pointing inaccuracies, multiple solutions, and round-off errors. None of these errors are known precisely. Thus, an experimental approach seems to be appropriate to determine the accuracy of the wind data.

The RMS errors in wind data measured by the smoke trail method were investigated by Camp and Scoggins [38]. They considered two wind profile measurements from the same smoke trail but used different camera pairs. Table B-I was extracted from their work. Errors associated with the profiles were determined from the differences between two profiles measured from the same trail using different camera pairs. Errors of individual wind speed measurements sometimes exceed 1 m/sec, but the RMS errors are believed to be generally below 0.5 m/sec as shown in Table B-I.

Errors in smoke trail wind data caused by vertical air motions have not been determined. Identification of points on the trail, which would be required for the measurement of vertical motions, has not been possible. It appears, however, that features of the smoke trail caused by large wind shears, thin layers of relatively fast wind speeds, etc., generally remain at about the same elevation, indicating that vertical air motions in these regions are small. Vertical air motions are believed to influence significantly only a very small percentage of the wind data measured by the smoke trail method.

TABLE B-I. RMS ERRORS (m/sec) IN SMOKE TRAIL WIND DATA OVER ALTITUDE INTERVAL 5-13 km FOR THREE PROFILES

Profile Number	V_x	V_y	V
1	0.17	0.32	0.27
2	0.27	0.61	0.60
3	0.16	0.43	0.27

REFERENCES

1. Killen, Gwendolyn L.: Balloon Behavior Experiments. USASRDL Technical Report 2093, US Army Signal Research and Development Laboratory, Fort Monmouth, New Jersey, 1960, p. 30.

2. Murrow, Harold N.; and Henry, Robert M.: Self-Induced Balloon Motions. Journal of Applied Meteorology, vol. 4, no. 1, 1965, pp. 131-138.

3. Schlichting, Hermann: Boundary Layer Theory. Fourth Ed., McGraw Hill Book Co., New York, 1960, pp. 1-40.

4. Goldstein, S.: Modern Developments in Fluid Dynamics. Vol. II, Oxford University Press, New York, 1938, pp. 481-503.

5. Bacon, D. L.; and Reid, E. G.: The Resistance of Spheres in Wind Tunnels and in Air. NACA Report No. 185, 1923, pp. 471-486.

6. Hoerner, S.: Tests of Spheres with Reference to Reynolds Number, Turbulence, and Surface Roughness. NACA Technical Memorandum No. 777, 1935, p. 30.

7. Platt, Robert C.: Turbulence Factors of N. A. C. A. Wind Tunnels as Determined by Sphere Tests. NACA Technical Report No. 558, 1936, pp. 283-303.

8. Dryden, Hugh L.; et al.: Measurement of Intensity and Scale of Wind-Tunnel Turbulence and Their Relation to the Critical Reynolds Number of Spheres. NACA Report No. 581, 1937, pp. 109-140.

9. Dryden, Hugh L.: Turbulence Investigations at the National Bureau of Standards. Proceedings of the Fifth International Congress of Applied Mechanics, 1938, pp. 362-367.

10. Roshko, Anatol: On the Drag and Shedding Frequency of Two-Dimensional Bluff Bodies. NACA Technical Note 3169, 1954, p. 29.

11. Fung, Y. C.: Fluctuating Lift and Drag Acting on a Cylinder in a Flow at Supercritical Reynolds Numbers. GM-TR-0165-00343, Space Technology Laboratories, Los Angeles, California, 1958, p. 45.

REFERENCES (Cont'd)

12. Preukschat, Werner A.: Measurements of Drag Coefficients for Falling and Rising Spheres in Free Motion. Aeronautical Engineering Thesis, California Institute of Technology, Pasadena, California, 1962, p. 76.

13. MacCready, Paul B.; and Jex, Henry R.: Study of Sphere Motion and Balloon Wind Sensors. NASA TM X-53089, 1964, p. 43.

14. Leviton, Robert: A Detailed Wind Profile Sounding Technique. Air Force Surveys in Geophysics, no. 140, AFCRL, 1962, pp. 187-195.

15. Scoggins, James R.: Aerodynamics of Spherical Balloon Wind Sensors. Journal of Geophysical Research, vol. 69, no. 4, 1964, pp. 591-598.

16. Scoggins, James R.: Spherical Balloon Wind Sensor Behavior. Journal of Applied Meteorology, vol. 4, no. 1, 1965, pp. 139-145.

17. Rogers, R. R. and Camitz, H. G.: Project Baldy - An Investigation of Aerodynamically-Induced Balloon Motions. Final Report, NASA Contract No. NAS8-11140, 1965, p. 80.

18. Reid, Daniel F.: Instability of Spherical Wind Sensing Balloons. Paper presented at AFCRL Scientific Balloon Symposium, Portsmouth, New Hampshire, 1964, p. 9.

19. Scoggins, James R.: An Evaluation of Detail Wind Data as Measured by the FPS-16 Radar/Spherical Balloon Technique. NASA Technical Note D-1572, 1963, p. 30.

20. Eckstrom, Clinton V.: Theoretical Study and Engineering Development of Jimsphere Wind Sensor. Final Report, NASA Contract No. NAS8-11158, 1965, p. 78.

21. Jiusto, James E.: High Resolution Wind and Wind Shear Measurement with Doppler Radar. Final Report, NASA Contract No. NAS8-1520, Cornell Aeronautical Laboratory, Inc., Buffalo, New York, 1962, p. 65.

22. Figge, E. E.; et al.: BALSA Balloon-Borne Sonic Anemometer. Technical Summary Report, NASA Contract No. NAS8-885, Cook Technological Center, Morton Grove, Ill., 1961.

REFERENCES (Cont'd)

23. Henry, Robert M.; et al.: The Smoke Trail Method for Obtaining Detailed Measurements of the Vertical Wind Profile for Application to Missile Dynamic Response Problems. NASA TN D-976, 1961.

24. Scoggins, James R.; and Susko, Michael: FPS-16 Radar/Jimsphere Wind Data Measured at the Eastern Test Range. NASA TM X-53290, 1965, p. 458.

25. Ryan, Robert S.; and Scoggins, James R.: The Use of Wind Shears in the Design of Aerospace Vehicles. Paper presented at 23rd meeting of the Structures and Materials Panel, AGARD, NATO, Paris, France, October 1966, p. 55.

26. Geissler, Ernst D.: Problems in Attitude Stabilization of Large Guided Missiles. Aerospace Engineering, October 1960, pp. 24-29; 68-72.

27. Danielsen, E. F.: Properties of Shear-Gravity and Inertial-Gravity Waves. Paper presented at joint AMS/AAAS meeting, Riverside, California, June 1965, p. 15.

28. Weinstein, A. I.; et al.: Mesoscale Structure of 11-20 km Winds. Journal of Applied Meteorology, vol. 5, no. 1, 1966, pp. 49-57.

29. Endlich, R. M.; et al.: Techniques for Determining a World-Wide Climatology of Turbulence Through Use of Meteorological Data. AFCRL-66-355, 1966, pp. 43-59.

30. Lamb, Sir Horace: Hydrodynamics. Dover Publications, 1932, pp. 123-124.

31. Hald, A.: Statistical Theory with Engineering Applications. John Wiley and Sons, New York, 1952, pp. 138-140.

32. Blackman, R. B.; and Tukey, J. W.: The Measurement of Power Spectra. Dover Publications, Inc., 1958, pp. 21-25.

33. Rogers, R. R.; and Camitz, H. G.: An Additional Note on Erratic Balloon Motions. Journal of Applied Meteorology, vol. 5, no. 3, 1966, pp. 370-373.

REFERENCES (Concluded)

34. McVehil, G. E.; et al.: Some Measurements of Balloon Motions with Doppler Radar. Journal of Applied Meteorology, vol. 4, no. 1, 1965, pp. 146-148.

35. Deming, Edward W.: Statistical Adjustment of Data. John Wiley and Sons, Inc., New York, 1943.

36. Houston, Charles: Detailed Wind Gusts and Shear Measurements from Photographs of Missile Exhaust Trails. NASA/MSFC MTP-M-COMP-3-60, 1960, p. 12.

37. Foster, Clyde: Smoke Trail Reduction Technique for Obtaining Wind Profiles. NASA TM X-53210, 1965, p. 29.

38. Camp, Dennis W.; and Scoggins, James R.: Some Practical Accuracy Considerations of Smoke Trail Wind Profile Data. NASA TM X-53261, 1965, p. 29.

"The aeronautical and space activities of the United States shall be conducted so as to contribute . . . to the expansion of human knowledge of phenomena in the atmosphere and space. The Administration shall provide for the widest practicable and appropriate dissemination of information concerning its activities and the results thereof."

—NATIONAL AERONAUTICS AND SPACE ACT OF 1958

NASA SCIENTIFIC AND TECHNICAL PUBLICATIONS

TECHNICAL REPORTS: Scientific and technical information considered important, complete, and a lasting contribution to existing knowledge.

TECHNICAL NOTES: Information less broad in scope but nevertheless of importance as a contribution to existing knowledge.

TECHNICAL MEMORANDUMS: Information receiving limited distribution because of preliminary data, security classification, or other reasons.

CONTRACTOR REPORTS: Scientific and technical information generated under a NASA contract or grant and considered an important contribution to existing knowledge.

TECHNICAL TRANSLATIONS: Information published in a foreign language considered to merit NASA distribution in English.

SPECIAL PUBLICATIONS: Information derived from or of value to NASA activities. Publications include conference proceedings, monographs, data compilations, handbooks, sourcebooks, and special bibliographies.

TECHNOLOGY UTILIZATION PUBLICATIONS: Information on technology used by NASA that may be of particular interest in commercial and other non-aerospace applications. Publications include Tech Briefs, Technology Utilization Reports and Notes, and Technology Surveys.

Details on the availability of these publications may be obtained from:

SCIENTIFIC AND TECHNICAL INFORMATION DIVISION

NATIONAL AERONAUTICS AND SPACE ADMINISTRATION

Washington, D.C. 20546